

A methodology for simultaneous retrieval of ice and liquid water cloud properties. Part 2: Near-global retrievals and evaluation against A-Train products

Odran Sourdeval,^{a*} Laurent C.-Labonnote,^b Anthony J. Baran,^c Johannes Mülmenstädt^a and Gérard Brogniez^b

^a*Institute of Meteorology, Universität Leipzig, Germany*

^b*Laboratoire d'Optique Atmosphérique, Université Lille 1, Villeneuve d'Ascq, France*

^c*Met Office, Exeter, UK*

*Correspondence to: O. Sourdeval, Universität Leipzig, Vor dem Hospitalore 1, D-04103 Leipzig, Germany.
E-mail: odran.sourdeval@uni-leipzig.de

This article is published with the permission of the Controller of HMSO and the Queen's Printer for Scotland.

This article presents results of a novel methodology capable of simultaneously retrieving optical and microphysical properties of multi-level ice and liquid clouds. The method was introduced in Part I, which theoretically demonstrated its capabilities, and its results are here analysed and evaluated against A-Train operational products. In addition to being robust to multi-layer conditions, another advantage of the method is that rigorous uncertainties and analysis tools are attached to its retrievals. Also, the combined use of short-wave and thermal infrared channels provides a wide range of sensitivity from moderately thin to thick ice cloud layers. Finally, the method is also novel in that the ice water path (IWP) is directly retrieved. These new retrievals should therefore be useful in providing new data for evaluating climate model predictions of IWP. In this study, our methodology has been applied to one year of A-Train measurements, narrowed to daytime conditions over oceanic surfaces. The retrievals and their uncertainties are statistically analysed, after a thorough discussion of the filtering process. It appears that our method is sensitive to IWPs ranging between about 0.5 and 1000 g m⁻², with uncertainties better than 25% between 5 and 500 g m⁻². Retrievals of the optical depth and effective radius of liquid layers have uncertainties better than 20%. Our retrievals are then compared to five independent operational A-Train products. Very good agreements, well within a factor of 2, are found by comparisons to products from active and passive instruments. These results overall lead to the validation of our method. Additionally, the robustness of passive operational products to multi-layer conditions is discussed. Preliminary comparisons show a possible overestimation of retrievals obtained under the single-layer approximation. A thorough assessment of this problem will be addressed in a following study.

Key Words: satellite retrievals; ice cloud; liquid cloud; multi-layer; A-Train; EarthCare; optimal estimation; remote sensing

Received 4 February 2016; Revised 14 June 2016; Accepted 25 July 2016; Published online in Wiley Online Library

1. Introduction

Clouds are a major concern to the climate research community due to their crucial role on the Earth's radiation budget (WCRP, 1986; Stephens, 2005; Baran, 2012). The Intergovernmental Panel on Climate Change (IPCC) has again highlighted, in its most recent report, the importance of reducing the current

uncertainties that remain with regard to cloud properties and processes (IPCC, 2013). Therefore it appears not only necessary to provide more accurate retrievals of cloud properties to the climate modeling community, but it is also critical to associate these retrievals with rigorous uncertainties and quality indicators.

The A-Train mission has proven to be highly valuable for providing a better understanding of the Earth's atmosphere,

thanks to unique possibilities of synergy between all kinds of active and passive instruments. The recent emergence of variational methods, such as the optimal estimation (e.g. Watts *et al.*, 1998; Rodgers, 2000), has also been particularly helpful for developing new retrieval methods which are capable of using the full range of A-Train measurements in order to retrieve a multitude of cloud properties (e.g. Austin *et al.*, 2009; Delanoë and Hogan, 2010; Deng *et al.*, 2012). Moreover, these methods have the advantage of associating rigorous uncertainties to their retrievals, and of providing useful tools for error and information content analysis (Rodgers, 1996). Such tools can be of great interest, not only for selecting retrievals in the optimal sensitivity range of a given set of measurements, but also for understanding and quantifying the capabilities and limitations of a retrieval methodology (e.g. L'Ecuyer *et al.*, 2006; Cooper *et al.*, 2006; Sourdeval *et al.*, 2013, 2015). This type of information analysis is therefore crucial for properly constraining the products of a retrieval method.

There exist nowadays numerous methods based on passive radiometric measurements which are capable of providing accurate retrievals of ice or liquid cloud properties (e.g. King *et al.*, 1998; Roebeling *et al.*, 2006; Garnier *et al.*, 2012, 2013). Yet, despite the non-negligible frequency of occurrence of multi-layer conditions between these two cloud types (e.g. Chang and Li, 2005a; Joiner *et al.*, 2010; Wind *et al.*, 2010), very few methods attempt simultaneous retrievals. As a consequence, assuming a single cloud layer in the atmospheric column not only implies fewer retrievals, which could affect climatologies in regions of high multi-layer occurrence, but it can also lead to retrieved properties and uncertainties which are substantially affected by the ignored ice or liquid cloud layer. Sourdeval *et al.* (2013), for instance, have shown, using an optimal estimation method together with information content theory, that an under-constrained liquid water cloud layer underneath the ice cloud can have a significant impact on retrievals and their uncertainties. These conclusions are in agreement with other recent studies, such as by Chang and Li (2005b) and Watts *et al.* (2011), which both show the potential impact of underlying liquid cloud layers on ice cloud retrievals from passive measurements and the benefit of attempting these multi-layer retrievals. Other studies, such as that by Davis *et al.* (2009), have similarly reported that retrievals of liquid cloud properties from radiometric measurements can also be strongly impacted by the presence of an ice cloud layer.

Following these conclusions, a novel methodology for simultaneous retrievals of ice and liquid cloud properties has been presented in the first part of the present study (Sourdeval *et al.*, 2015). This methodology uses information from a set of five passive measurement channels, ranging from the visible to the thermal infrared, in order to retrieve integrated properties of each cloud layer. The use of a variational method associated with information theory also ensures that retrievals are provided together with rigorous uncertainties and useful analysis tools, such as the cost function or degrees of freedom. In Part I, several information content analyses were performed and demonstrated the theoretical capabilities of the method in multi-layer situations. These analyses clearly showed that the methodology should be perfectly capable of simultaneously retrieving the ice water path of one ice cloud layer and the optical depth and droplet effective radius of one liquid cloud layer in a wide range of multi-layer conditions. Moreover, in agreement with results from Cooper *et al.* (2007), the selected five-channel measurement vector should be particularly efficient for retrieving the ice water path of optically thin and thick ice cloud layers, as it merges the advantages of the commonly used split-window (Inoue, 1985) and NK (Nakajima and King, 1990) bi-spectral approaches.

Sourdeval *et al.* (2015) have briefly verified these theoretical expectations by using a short case-study containing *in situ* observations, but global retrievals and further comparisons to operational products remain necessary for a thorough evaluation of the method. Therefore the present article, which constitutes the

second part of the study, presents the results of this evaluation. The multi-layer retrieval methodology is applied to one year of near-global A-Train measurements, i.e. over an oceanic surface, in daytime conditions and excluding high-latitude regions. These retrievals are first statistically analysed before being compared to a multitude of independent active and passive operational A-Train products for validation purposes. The impact of multi-layer conditions on several of these operational products is also discussed.

The article is organised as follows. Section 2 presents the retrieval methodology through a detailed description of the state and measurement vectors. The process of identifying cloud layers and the impact of the vertical homogeneity assumption on cloud retrievals are also discussed. Section 3 thoroughly details how the dataset has been filtered in order to remove retrievals which do not allow a sufficient coherence between the forward model and the measurements, or which are too dependent on *a priori* assumptions. This section also discusses the selection and the spatial distribution of several types of scene which have been selected to conduct the study. Near-global retrievals are then presented in section 4 in the form of probability density functions and spatial distributions. These retrievals and their associated uncertainties are subsequently statistically analysed. Section 5 compares retrievals from our multi-layer methodology to those of five A-Train operational products. Such comparisons aim primarily at validating our retrievals, but can also serve to observe the robustness of some passive A-Train products to double-layer conditions. Finally, the main results of this study are summarized in section 6.

2. The multi-layer (ML) methodology

The results presented in this study are based on a methodology for multi-layer retrievals developed by Sourdeval *et al.* (2015) (hereafter S15). This method uses a set of radiometric measurements, spectrally ranging from the visible to the thermal infrared, to simultaneously retrieve integrated properties of ice and liquid water clouds. It is based on a variational scheme which uses the optimal estimation method in order to associate retrievals with rigorous uncertainties and useful analysis tools (Rodgers, 2000).

It should be noted that this retrieval method currently is constrained to the A-Train track due to its need of active instruments for identifying and positioning cloud layers, as later explained in section 2.1. In order to avoid strong uncertainties associated with the surface albedo, the ML methodology is for the moment limited to retrievals over oceans and out of high-latitude regions (i.e. above 60°N and below 60°S). The use of visible and near-infrared channels also narrows its retrievals of liquid cloud properties to daytime conditions.

This article aims to evaluate how the methodology presented in S15 can be applied on a near-global scale, which implies that minimal modifications are intended to the original method. However the processes of cloud layer identification and error calculation on the cloud-top altitude have been modified in order to better fit the needs of this study. Rigorous uncertainties associated with the vertical homogeneity assumption of the ice cloud layer have also been implemented. These updates are presented in this section, along with a detailed description of the state and measurement vectors. A full description of the retrieval methodology is not intended here, as it has already been thoroughly provided by S15.

2.1. Identification of cloud layers

In S15, the ML methodology uses the scene classification product provided by the Cloud-Aerosol Lidar with Orthogonal Polarization (CALIOP) operational algorithm in order to identify and distinguish between three main cloud types: ice (classified by CALIOP as cirrus or deep convective), *mid* liquid (classified as

altostratus or altocumulus) or *low* liquid (classified as cumulus, stratus or stratocumulus). CALIOP discriminates the cloud phase by using the lidar linear depolarization ratio and the temperature, while the cloud classification is obtained using the pressure, opacity and cloud fraction of each layer (Liu *et al.*, 2005). However such a classification can appear limited for the purpose of multi-layer retrievals because of the complete attenuation of CALIOP's laser pulse at cloud optical depths between about 3 and 5 (Sassen *et al.*, 2008; Winker *et al.*, 2010). It also offers no clear discrimination of mixed-phase cloud layers (typically where a liquid/supercooled top overlaps the ice), which can contaminate the retrievals (Hu *et al.*, 2009). For these reasons, the cloud identification method has been modified.

The updated version of the ML methodology makes use of a combined radar–lidar product, DARDAR*-MASK (version 1.1.4) (Delanoë and Hogan, 2010; Ceccaldi *et al.*, 2013), in order to set up the cloud profiles which are utilised for the retrievals. This product provides profiles of categorised atmospheric features with a vertical resolution of 60 m. The phase of each cloud layer is obtained using the CALIOP backscatter coefficient and the CloudSat Cloud Profiling Radar (CPR) reflectivity. The latter is particularly helpful for identifying liquid cloud layers in multi-layer conditions where the lidar pulse is completely attenuated by an ice layer. DARDAR-MASK can therefore distinguish between three main cloud types within the same atmospheric column: ice, mixed-phase, and liquid.

2.2. The state vector

The single-scattering properties of ice crystals are provided by a new parametrization, developed by Baran *et al.* (2014), which expresses these properties as function of the ice water content (IWC) and the in-cloud atmospheric temperature (T_c). This parametrization is based on a mixture of roughened ice crystal habits (Baran and Labonnote, 2007), which is integrated over particle size distributions (PSD) estimated as functions of IWC and T_c using the moment estimation parametrization developed by Field *et al.* (2007). Consequently, providing a temperature profile (here from reanalyses of the Global Modeling and Assimilation Office (GMAO)), this parametrization allows the IWC alone to provide all necessary information for radiative transfer simulations. This implies that the ice water path (IWP, or vertically integrated IWC) can directly be retrieved without referring to conventional relationships between the cloud optical depth (OD) and the vertically averaged ice crystal effective radius (R_e). Such direct retrievals can be advantageous due to possible ambiguities in the concept of effective radius for ice clouds (Mitchell, 2002), but also to the current need for rigorous IWP retrievals for parametrizing or evaluating ice schemes in climate models, where this parameter is linked to prognostic variables (e.g. Tiedtke, 1993; Morrison and Gettelman, 2008). Nevertheless it should be noted that the ice cloud OD can still be inferred from the retrieved IWP and an in-cloud temperature profile. More details on this parametrization and on the calculation of OD for ice clouds can be found in the Appendix. As a consequence, the IWP alone is used for describing ice clouds in the state vector, while liquid clouds are described by the more traditional OD and R_e couple.

In S15, the methodology distinguishes between two liquid cloud layers, referred to as *low* and *mid* in order to distinguish between their positions in the troposphere. The use of two separate liquid layers, whose OD and R_e have to be retrieved, was then justified to perform a thorough analysis of the theoretical capabilities and limitations of the retrieval method. However, these analyses were idealized and the presence of two liquid cloud layers in the state vector no longer seems justified in the context of actual retrievals. Yet, this mid-level layer can still be seen as a convenient

way to denote the presence of mixed-phase clouds (identified by DARDAR-MASK) in the atmospheric column. Ignoring their presence, and more particularly their supercooled liquid top, could otherwise strongly impact retrievals of ice cloud properties (Sourdeval *et al.*, 2013). Hence, retrieving an optical depth for such a layer should be attempted in order to improve IWP retrievals in double-layer conditions. Because their supercooled liquid top is likely to dominate the absorption in infrared channels, and in the absence of a better microphysical description, mixed-phase layers are here approximated as being being fully liquid. This approximation seems reasonable for correcting IWP retrievals, but not for providing accurate properties of mixed-phase cloud layers or of possible liquid clouds lying underneath. Such cases will therefore not be analysed in this study, as further discussed in section 3.

The state vector \mathbf{x} is therefore

$$\mathbf{x} = \begin{pmatrix} \ln(\text{IWP}) \\ \ln(\text{OD}_{\text{liq}}) \\ \ln(R_{e,\text{liq}}) \\ \ln(\text{OD}_{\text{mix}}) \\ \ln(R_{e,\text{mix}}) \end{pmatrix}, \quad (1)$$

where the subscripts liq and mix indicate that the optical depth and effective radius correspond to liquid and mixed-phase layers, respectively. It should be kept in mind that mixed-phase cloud properties are only introduced in the state vector as an attempt to improve IWP retrievals in double-layer conditions, and that these are separated from low liquid cloud properties for reasons of clarity. The *a priori* state vector used in S15 has also been adapted to the needs of near-global retrievals by widening the range of probable *a priori* solutions. This is desired in order to avoid strong dependencies on any *a priori* consideration. It can be noted that the absence of a cloud layer in the atmospheric profile is treated by setting the corresponding IWP or OD to zero, associated with extremely low uncertainties in the *a priori* state error covariance matrix.

2.3. The measurement vector

The necessary information for an optimal retrieval of the state vector is provided by a set of five radiometric measurement channels, which constitute the measurement vector \mathbf{y} :

$$\mathbf{y} = \begin{pmatrix} R_{8.6}^{\text{IIR}} \\ R_{10.6}^{\text{IIR}} \\ R_{12.0}^{\text{IIR}} \\ R_{0.85}^{\text{MODIS}} \\ R_{2.13}^{\text{MODIS}} \end{pmatrix}, \quad (2)$$

where $R_{8.6}^{\text{IIR}}$, $R_{10.6}^{\text{IIR}}$, and $R_{12.0}^{\text{IIR}}$ are the Infrared Imaging Radiometer (IIR) radiances measured at 8.65, 10.60, and 12.05 μm , respectively, and $R_{0.85}^{\text{MODIS}}$ and $R_{2.13}^{\text{MODIS}}$ are the MODerate Resolution Imaging Spectroradiometer (MODIS) reflectances measured at 0.85 and 2.13 μm , respectively. MODIS measurements have been collocated to those of IIR through the use of the CALIOP-Track (CALTRACK) reanalysis products provided by the ICARE data centre (Pascal and Manley, 2009). Cooper *et al.* (2007) have initially shown the benefit of using such a five-channel measurement vector for retrieving ice cloud properties, as it combines the advantages of the two commonly used bi-spectral techniques: the split-window (Inoue, 1985) and NK (Nakajima and King, 1990) methods, respectively sensitive to optically thinner and thicker ice clouds. These recommendations were confirmed by S15, who have theoretically demonstrated that this set of channels should allow accurate retrievals of liquid and ice cloud properties in most single- and double-layer conditions. The use of five channels, even in single-layer conditions, also has the advantage of ensuring that the retrievals are spectrally coherent and therefore better constrained.

*raDAR/liDAR.

2.4. Discussion on the vertical homogeneity assumption

The ML methodology follows the vertical homogeneity assumption for describing ice and liquid cloud layers (i.e. the vertical distribution of their properties is considered to be homogeneous). However, global observations indicate that the size and water content of ice crystals vertically evolve due to aggregation processes (e.g. Ham *et al.*, 2013; Feofilov *et al.*, 2015), and an erroneous representation of these profiles can have significant effects on ice cloud retrievals or radiation (e.g. Yang *et al.*, 2001, 2012). More particularly, Zhang *et al.* (2010) have shown that vertical inhomogeneities can differently impact IWP retrievals depending on whether they are based on bi-spectral approaches using thermal infrared radiances (split-window) or visible and NIR reflectances (NK). Because ML merges both of these methods, inconsistencies during the retrieval process are expected for thick clouds if, at minimum, uncertainties are not rigorously associated with the shape of the vertical IWC profile.

Indeed, a recent assessment study by Feofilov *et al.* (2015) has shown that the vertical profile of IWC in thick ice clouds tends to peak towards the cloud base in the shape of a trapezoidal or low triangular distribution. This study also concludes that using a constant IWC profile in retrieval methods is only reasonable for $IWP < 100 \text{ g m}^{-2}$. At higher values, S15 have shown that the information provided by thermal infrared channels on the IWP saturates above about 130 g m^{-2} , but that the visible channel can still be used for retrievals. This is a direct consequence of the low influence of absorption processes at visible wavelengths, which also implies a lack of sensitivity of the $0.85 \mu\text{m}$ channel to vertical inhomogeneities (Yang *et al.*, 2001). However, at high IWPs, the vertical homogeneity assumption causes the entire cloud layer to nearly become a black body in the thermal infrared spectrum, and consequently the forward model simulates brightness temperatures (or corresponding radiances) close to the cloud-top temperature. On the other hand, if the IWC of the observed cloud is in fact concentrated towards the cloud-base altitude, thermal infrared measurements will correspond to warmer brightness temperatures resulting from absorption deeper in the cloud. This incoherence between measurements and forward model simulations will lead to an abnormally high value of the cost function (cf. section 3.2) and, as a result, perturb our iterative Levenberg–Marquardt minimization scheme or create a failure in the retrievals. Subsequently, no accurate retrieval of IWP for thick ice clouds can be expected from our five-channel methodology, unless (i) a realistic vertical IWC profile is utilised for the retrievals, or (ii) uncertainties associated with vertical inhomogeneities are accounted for to encompass the above-mentioned deviation between forward model simulations and measurements in infrared channels.

For the needs of this study, additional rigorous uncertainties have been associated with the forward model. To that end, the deviation between simulations obtained using vertical homogeneity and a low triangular shape profile is included in the measurement error variance–covariance matrix. This particular shape appears reasonable for uncertainty calculations as it represents the most extreme and dominant shape observed by Feofilov *et al.* (2015) when $IWP > 100 \text{ g m}^{-2}$. In our study, it corresponds to a profile where the IWC linearly decreases from 0 to IWC_{max} , whose value is calculated so that the vertical integral of the IWC profile matches the IWP. It should be noted that this uncertainty does not only account for the vertical inhomogeneity of IWC but also of ice crystal habits, which become increasingly complex as IWC and T_c increase towards the cloud base (Baran *et al.*, 2014). We recall that this is made possible as ML divides each cloud layer into 100 m sub-layers. Additionally, it appears that the cloud-top altitude provided by lidar–radar information may be too constraining in the case of very thick ice clouds, where the cloud top is only representative of extremely small IWC values. In order to make

our retrieval method less dependent on lidar–radar input in these situations, the current uncertainty associated with the cloud-top altitude (100 m) has been replaced by 20% of the total cloud thickness.

It can be noted that such uncertainties may limit double-layer retrievals to IWPs less than about 130 g m^{-2} . Nevertheless, this consequence is acceptable in this study since, as later shown in section 5.4 using active operational products, multi-layer conditions are dominated by ice clouds with IWPs less than this threshold.

Finally, it should be kept in mind that effects due to ice cloud horizontal (e.g. Fauchez *et al.*, 2015) and liquid cloud horizontal and vertical (e.g. Platnick, 2000; Zhang *et al.*, 2012) heterogeneities are not taken into account in this study. These will require a substantial modification of the ML methodology, such as for instance the use of a more realistic liquid cloud model (e.g. Brenguier *et al.*, 2000; Schüller *et al.*, 2005).

3. Selection of an optimal dataset

The use of optimal estimation has the strong advantage that retrievals are provided not only along with rigorous uncertainties but also with a wide range of useful analysis tools, such as the Shannon information content, total and partial degrees of freedom (DOF), and the cost function. The last two have been used in this study to filter out ill-retrieved parameters from the ML dataset, i.e. to identify when retrievals are strongly impacted by *a priori* considerations or do not allow the forward model to be coherent with the measurements. The analyses presented in this article have also been narrowed down to a few relevant types of scene. This section thoroughly describes this data selection process.

3.1. Types of scene

Three cloud layers can be included in the ML methodology (i.e. ice, mixed-phase and liquid), which means that a total number of seven types of scene can potentially occur (from single- to triple-layer). However, as discussed in section 2.2, mixed-phase cloud layers are only included as a correction for IWP retrievals, and so their properties are not taken into account in this study. Additionally, because of the inaccurate microphysical representation of mixed-phase clouds, retrievals of liquid cloud properties could be erroneous underneath a mixed-phase layer and are therefore not considered. Consequently, types of scene corresponding to single mixed-phase, double mixed-phase + liquid, and triple-layer have been removed from the analyses presented here.

An analysis of the cloud information extracted from DARDAR-MASK shows that single-layer cloud cases represent about 80% of the total cloud fraction, with about 32% of single ice cloud layers, and 28% and 20% of single liquid and mixed-phase cloud layers, respectively. Therefore, nearly 20% of the analysed cloud cover corresponds to multi-layer types of scene, dominated by ice + liquid (10%) and ice + mixed-phase (6%) double-layer scenes. Moreover, about 33% of the total ice cloud cover corresponds to a double ice + liquid/mixed-phase type of scene, while about 26% of liquid clouds are overlapped by an ice layer. These numbers are in global agreement with existing climatologies on multi-layer cloud conditions, which nevertheless remain highly variable depending on the instrumentation being used (e.g. Wang *et al.*, 2000; Heidinger and Pavolonis, 2005; Joiner *et al.*, 2010).

However, the occurrence of multi-layer types of scene strongly depends upon location. Figure 1(a) shows the spatial distribution of the total cloud fraction used for ML retrievals, averaged over a $2^\circ \times 2^\circ$ latitude–longitude box grid. Figure 1(b)–(d) represent the cloud fraction corresponding to each type of scene treated in this study, i.e. single ice, single liquid, double ice + liquid/mixed-phase types of scene, respectively. Figure 1(e)

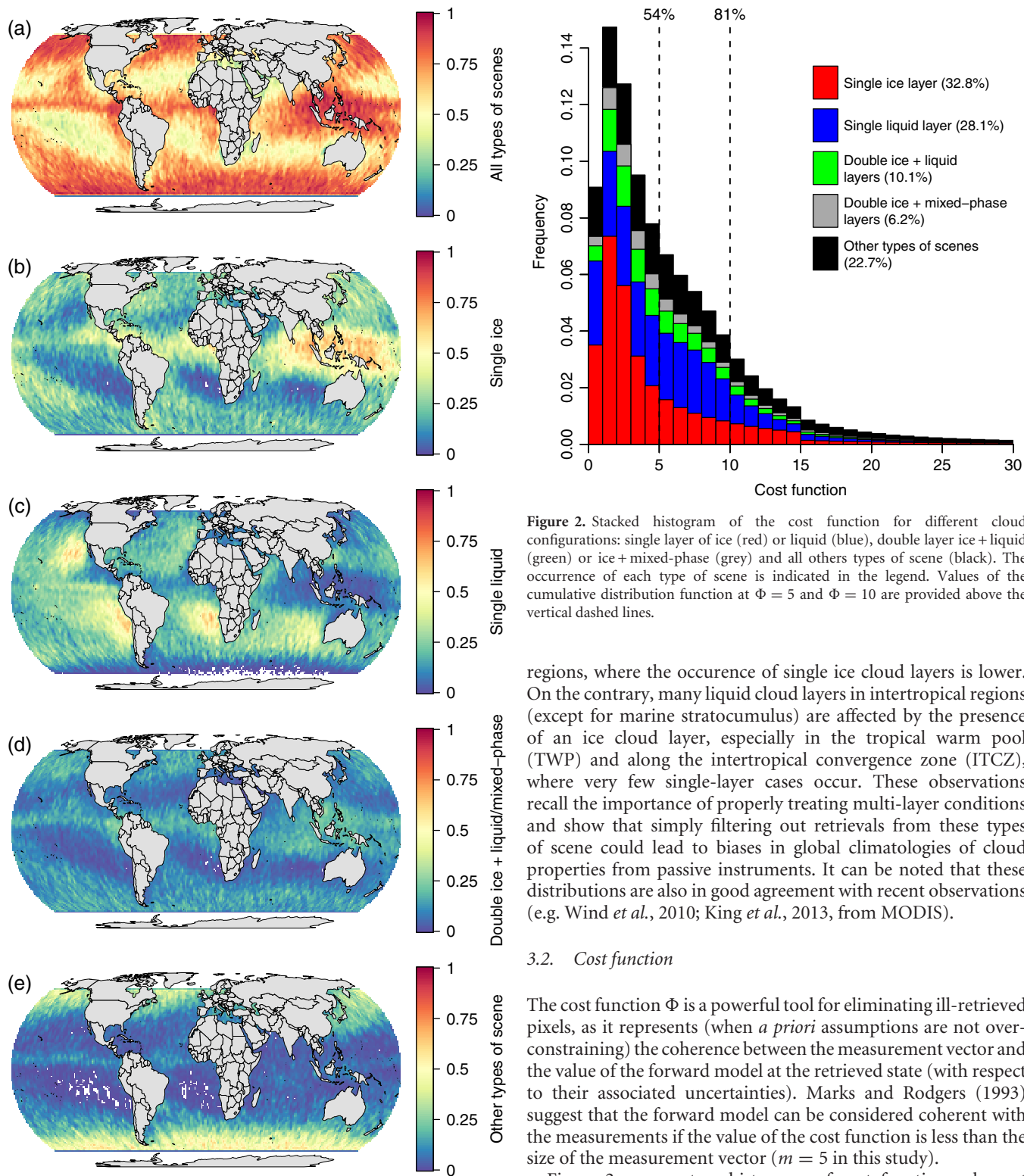


Figure 1. (a) Spatial distribution of the cloud fraction identified by DARDAR-MASK and corresponding to ML retrievals for the year 2008, and fraction of (b) single ice cloud layers, (c) single liquid cloud layers and (d) double ice + liquid/mixed-phase cloud layers. Panel (e) shows the fraction of cloud layers excluded from the ML dataset.

shows the distribution of the excluded types of scene. It can be observed that double-layer cases between ice and liquid/mixed-phase clouds are homogeneously distributed in areas of high cloud fraction, where they cover between 20 and 30% of the globe. Also, nearly 50% of cloud cases near high latitudes will not be treated in this study due to the high occurrence of single mixed-phase cloud layers. Figure 1 shows that ice cloud layers are, in absolute terms, homogeneously impacted by the presence of liquid clouds all over the globe. Consequently, a higher relative occurrence of multi-layer conditions is found in midlatitude

Figure 2. Stacked histogram of the cost function for different cloud configurations: single layer of ice (red) or liquid (blue), double layer ice + liquid (green) or ice + mixed-phase (grey) and all others types of scene (black). The occurrence of each type of scene is indicated in the legend. Values of the cumulative distribution function at $\Phi = 5$ and $\Phi = 10$ are provided above the vertical dashed lines.

regions, where the occurrence of single ice cloud layers is lower. On the contrary, many liquid cloud layers in intertropical regions (except for marine stratocumulus) are affected by the presence of an ice cloud layer, especially in the tropical warm pool (TWP) and along the intertropical convergence zone (ITCZ), where very few single-layer cases occur. These observations recall the importance of properly treating multi-layer conditions and show that simply filtering out retrievals from these types of scene could lead to biases in global climatologies of cloud properties from passive instruments. It can be noted that these distributions are also in good agreement with recent observations (e.g. Wind *et al.*, 2010; King *et al.*, 2013, from MODIS).

3.2. Cost function

The cost function Φ is a powerful tool for eliminating ill-retrieved pixels, as it represents (when *a priori* assumptions are not over-constraining) the coherence between the measurement vector and the value of the forward model at the retrieved state (with respect to their associated uncertainties). Marks and Rodgers (1993) suggest that the forward model can be considered coherent with the measurements if the value of the cost function is less than the size of the measurement vector ($m = 5$ in this study).

Figure 2 represents a histogram of cost function values at the end of retrievals, where the contributions from different types of scene are stacked. It can be seen that most single-layer cases of ice clouds (red) are associated with $\Phi < 5$ and can therefore be considered well retrieved with regards to their radiative coherence with the observations. Single-layer cases of liquid clouds (blue) show higher cost function values, with a high occurrence until about $\Phi = 10$. A high cost function can indicate inadequate approximations in the forward model, an underestimation of measurement uncertainties or over-constrained *a priori* assumptions. It appears in our case that more than 50% of single-layer liquid cloud retrievals with $\Phi > 5$ correspond to thin clouds of OD less than 2 (not shown here), which could mean a small inconsistency in the oceanic properties used by the forward model for simulating the visible channel. However this has little impact on the analyses presented in this study since the ML methodology is not very sensitive to

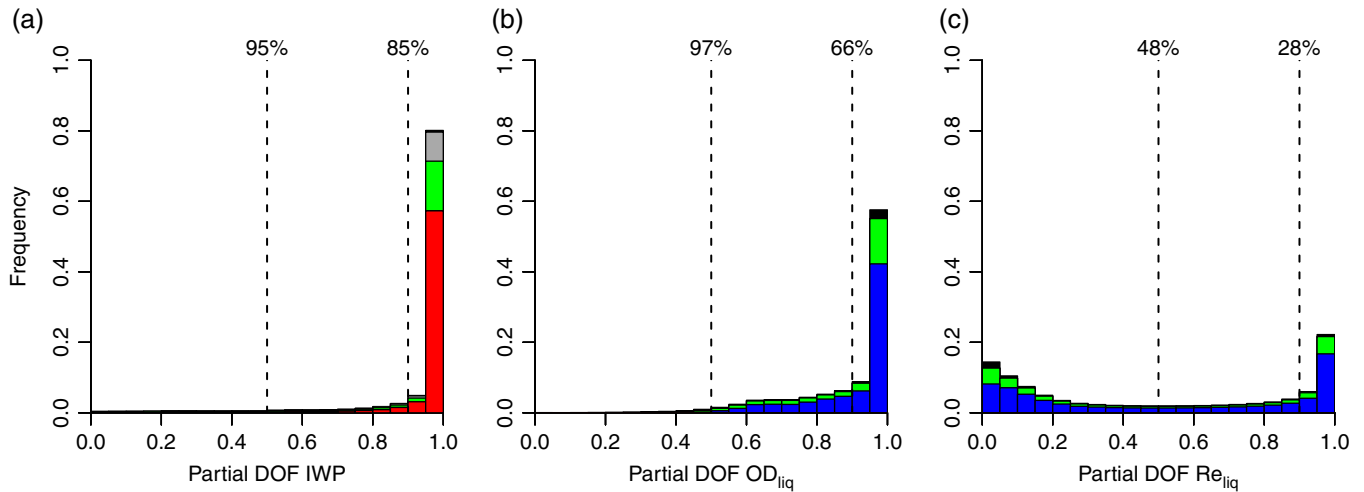


Figure 3. Stacked histogram of the partial DOFs corresponding to retrievals of (a) IWP, (b) OD_{liq} and (c) Re_{liq} obtained in different cloud configurations. The colour code follows that of Figure 2. Values of the complementary cumulative distribution function at 0.5 and 0.90 are provided above vertical dashed lines.

such thin liquid clouds, as shown by S15 and discussed in section 3.3. Retrievals obtained in double-layer conditions (green and grey) are globally associated with a small value of the cost function, which shows that the properties of both layers are consistent with each other and radiatively coherent with all the measurements. This is also reassuring in the fact that the approximation of treating mixed-phase layers as being fully liquid seems to provide coherent results for the needs of this methodology. Finally, Figure 2 indicates that about 54% of the retrievals satisfy the $\Phi < m$ condition, while 81% have a cost function $< 2m$. An upper threshold of $\Phi_{max} = 2m$ could be useful to account for possible under-constrained uncertainties on forward model parameters while still requesting a reasonable convergence between simulations and observations.

3.3. Degrees of freedom

Total degrees of freedom represent the amount of independent pieces of information available in the measurement vector in order to retrieve the entire state vector. Its value ranges between 0 and the size of the state vector (n), where 0 means an absence of information and n indicates that full information is obtained on each component of \mathbf{x} . Furthermore, the total DOF can be split into partial DOFs in the state or measurement spaces (Rodgers, 1996). Partial DOFs in the state space would for instance provide the amount of information contained by the whole measurement vector on each individual component of \mathbf{x} . Further details on this process and how it is applied to the ML methodology can be found in S15. A parameter that is retrieved with a partial DOF of 1 suggests that the measurements have carried enough information for its optimal retrieval, whereas a partial DOF of 0 would indicate that the information has fully been provided by *a priori* assumptions. A partial DOF of 0.5 corresponds to the signal-to-noise level.

Stacked histograms of partial DOFs associated with retrievals of IWP, OD_{liq} and Re_{liq} are presented in Figure 3(a)–(c), respectively, where the colour legend follows that of Figure 2. Figure 3(a) shows that high values of partial DOFs are attributed to IWP retrievals, which indicates that very strong information is available on this parameter. More than 95% of IWP retrievals are indeed associated with a partial DOF greater than the signal-to-noise level and 85% with partial DOFs greater than 0.90. A lower limit of 0.90 is interesting, as it ensures that at least 90% of the information has been provided by the measurements and therefore that retrievals are not significantly affected by *a priori* assumptions. Figure 3(b) shows that high values of partial DOFs are also associated with retrievals of OD_{liq} . Nearly all of them have partial DOFs > 0.5 and 66% are above 0.90. On the contrary, partial DOFs attributed to Re_{liq} retrievals are much lower, as indicated in Figure 3(c).

It appears that 48% of them are above the signal-to-noise level and only 28% are greater than 0.90, which shows a strong lack of information on this parameter in most cases. Finally, it is also observed in Figure 3 that the value of partial DOFs does not strongly depend on the type of scene.

In order to understand these distributions better, the partial DOFs on IWP, OD_{liq} and Re_{liq} in multi-layer conditions are represented as functions of OD_{liq} and IWP in Figure 4(a)–(c), respectively. As expected, Figure 4(a) shows very high information associated with IWP retrievals, almost independently of OD_{liq} , with partial DOFs generally higher than 0.90 and between IWP values of about 1 and 130 g m^{-2} . Figure 4(b) shows that the information content is also high on the liquid cloud OD, provided that the OD is greater than about 2 and that the ice layer is not too thick. The apparent decrease in partial DOF values around $OD \simeq 8.5$ at high IWPs corresponds to an artefact caused by situations where OD_{liq} lacks information to be retrieved and therefore returns or stays close to its *a priori* value. The same observation logically appears on the partial DOF associated with Re_{liq} retrievals, presented in Figure 4(c), since a lack of information on OD_{liq} usually implies a lack of information on Re_{liq} . Figure 4(c) also shows that Re_{liq} starts lacking information when the OD_{liq} is less than about 8 or when the IWP is greater than about 60 g m^{-2} . The signal-to-noise level is reached at $OD_{liq} \simeq 4$. Considering that most liquid clouds have an OD less than this value, as later shown in section 4.1, this explains why very few Re_{liq} retrievals are associated with a high partial DOF. It should be noted that Figure 4 perfectly reflects the theoretical expectations from S15.

3.4. Summary on the filtering process

Three different types of filtering have been applied to the ML dataset: a type of scene filter that removes the presence or bad impact of mixed-phase cloud layers, a cost function filter that ensures that the retrievals allow forward model simulations to be consistent with the measurements, and a degree of freedom filter that avoids the influence of *a priori* assumptions on the retrievals.

Figure 5 summarises how the overall filtering process impacts the ML dataset by providing the amount of rejected retrievals of IWP (left block of histograms), OD_{liq} (middle) and Re_{liq} (right). Several threshold combinations have been considered for filtering the data and are distinguished by a colour code. The filtering can be considered loose ($\Phi_{max} = 10$ and $DOF_{min} = 0.5$, in green), strong ($\Phi_{max} = 5$ and $DOF_{min} = 0.90$, in blue), or a mixture of both (in red and orange). The stacked histograms also indicate what type of filtering causes the rejection of the dataset, through the use of different hatching patterns. A vertical hatching means

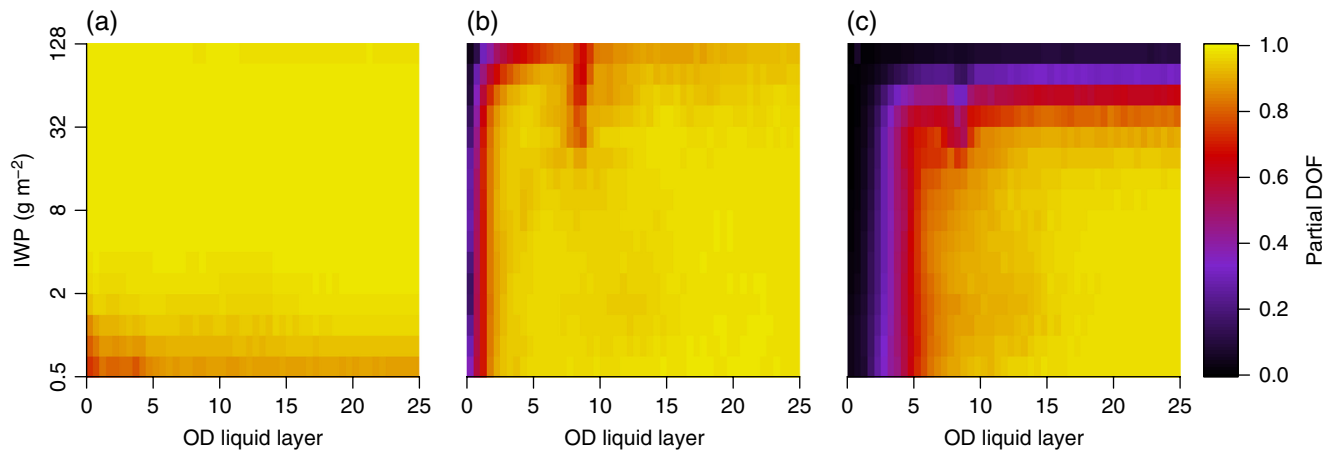


Figure 4. Partial DOFs corresponding to retrievals of (a) IWP, (b) OD_{liq} and (c) R_{eliq} as functions of OD_{liq} and IWP in multi-layer conditions.

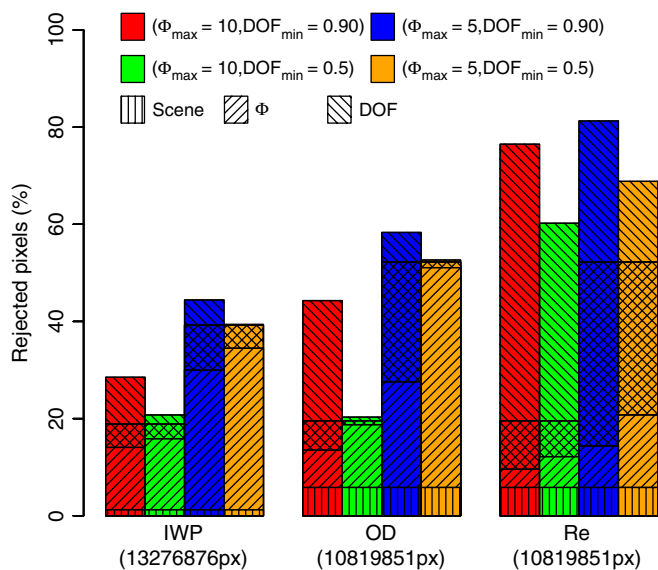


Figure 5. Stacked histograms representing the percentage of rejected retrievals of IWP (left), OD_{liq} (middle) and R_{eliq} (right) for several couples of Φ and partial DOF thresholds, as indicated by the colour legend. Different hatching patterns in the stacked histograms indicate the cause for rejection: wrong type of scene (vertical), high Φ (right), low partial DOFs (left) or both high Φ and low partial DOFs (crossed). The total number of retrievals before filtering is indicated under the histogram of each retrieved parameter.

that the rejection is caused by a wrong type of scene, a right hatching that the cost function is higher than its threshold, a left hatching that the partial DOF is lower than its threshold. A crossed hatching therefore means that the last two occur simultaneously. The total number of retrievals before filtering is indicated under each histogram and corresponds to about 13.3 and 10.8 million pixels for ice and liquid cloud properties, respectively. It can first be observed in Figure 5 that, depending on the choice of threshold, the rejection rate is about 20–45% for IWP retrievals, 20–60% for OD_{liq} retrievals, and 60–80% for R_{eliq} retrievals. These numbers prove again the importance of using the cost function and degrees of freedom, which dominate the filtering process. For instance, without these tools, at least 55% of R_{eliq} retrievals otherwise included in the analysed dataset would have been contaminated by strong *a priori* assumptions (partial DOF less than 0.5) and/or would cause the forward model to be largely incoherent with the observations (Φ greater than 10). Out of the loose filtering case, it appears that other threshold combinations lead to percentages of total rejected pixels within about 10–20% of each other. The threshold combination therefore does not appear critical so long as either the DOF or the Φ filtering is strong enough. Since the filtering on the cost function concerns the full set of retrievals at once and can be impacted by inaccuracies in the forward model,

the looser threshold of $\Phi_{max} = 10$ is taken for this study. However, in order to remove any significant *a priori* assumptions from the retrievals, the stronger threshold $DOF_{min} = 0.90$ is selected. The average amount of rejected retrievals therefore is about 30% for the IWP, 45% for OD_{liq} and 75% for R_{eliq} . Despite these strong rejection rates, the high number of retrievals should allow the results presented in this study to be statistically significant.

Complementing the above, Figure 6 shows the spatial distribution of the rejection rate (i.e. the normalized amount of rejected retrievals in a $2^\circ \times 2^\circ$ box grid) due to the selected threshold. The total rejection rate is presented in Figure 6(j)–(l) and the contributions of the scene type, cost function, and DOF filterings are indicated in Figure 6(a)–(c), (d)–(f) and (g)–(i), respectively. It is worth noting that the sum of all contributions does not necessarily equal the total rate since cost function and partial DOF filterings can happen simultaneously. The rejection rate of IWP, OD_{liq} , and R_{eliq} retrievals is shown in the first, second, and third rows, respectively. As expected from Figure 1, the type of scene filter mainly is significant towards high latitudes, where double-layer conditions between liquid and mixed-phase clouds occur more frequently, but also along the ITCZ. The rejection of IWP due to cost function filtering is on the contrary more evenly distributed, with about 25%, except for subsidence regions where ice clouds occur less. Regarding liquid clouds, high rejection rates due to the cost function filtering are found in intertropical open oceanic regions, and particularly in the TWP where it can reach 50%. These observations are very consistent with those of Cho *et al.* (2015), who have precisely analysed the failure rate in MODIS marine liquid cloud retrievals. In that study, failure is decided when no OD_{liq} and R_{eliq} combination within the MODIS look-up table can explain the measurements, which is comparable to our cost function test. A failure rate up to 40% is also observed in these regions and is mainly attributed to sub-pixel inhomogeneities and viewing geometries. Finally, the DOF filtering is substantial in regions where clouds are too thin for measurements to bring sufficient information (cf. Figure 8). These correspond to southern subsidence regions for the IWP and open oceanic trade wind cumuli regions for OD_{liq} and R_{eliq} . Overall, it is noticed that the spatial distribution of IWP rejected retrievals is relatively homogeneous (around 30%), except for southern subsidence regions where it can reach 60%. The rejection of OD_{liq} retrievals can reach 75% in trade-wind regions, but is less than 30% in stratocumulus and midlatitude regions. R_{eliq} retrievals have a rejection rate higher than 80% in regions where the OD_{liq} is also highly rejected, and of about 50% for stratocumulus and midlatitude clouds.

This type of analysis not only helps at filtering data but is also extremely useful for better understanding the limitations of retrieval methods. For instance, a high cost function due to cloud sub-pixel inhomogeneities could be lowered if the latter are better represented in the forward model or its uncertainties (e.g.

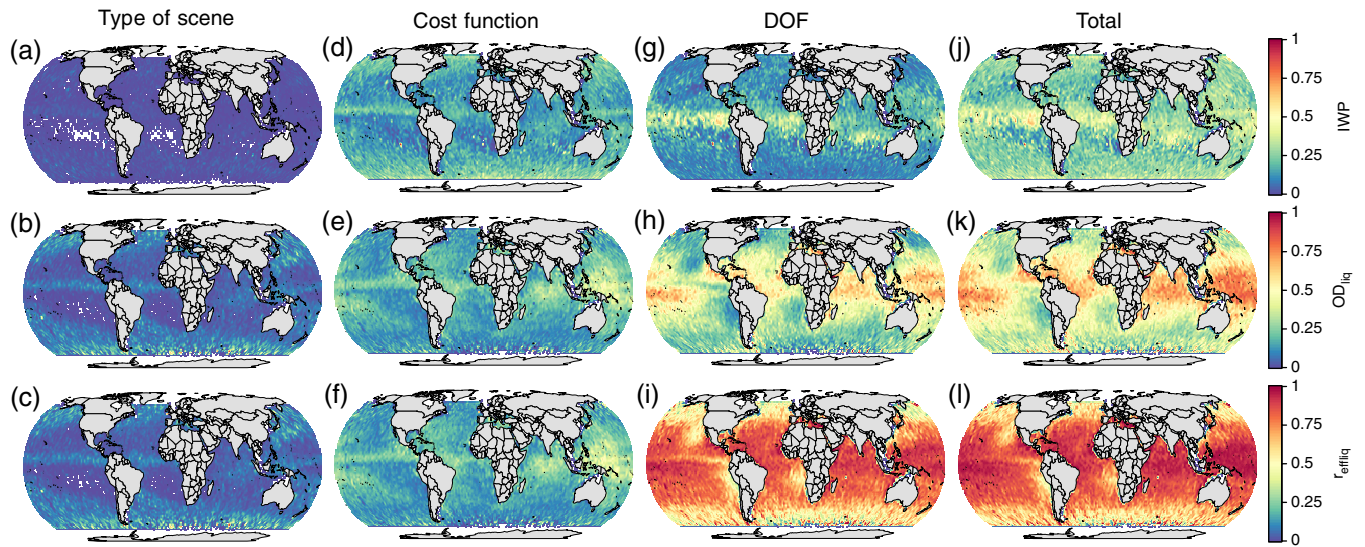


Figure 6. Spatial distribution of the rejection rate due to a (a–c) type of scene, (d–f) cost function, and (g–i) partial DOF filtering, using with the selected $\Phi_{\max} = 10$ and $\text{DOF}_{\min} = 0.90$ thresholds. The total rejection rate (j–l) is obtained when all filters are simultaneously applied. Rejection rates are shown separately for the (a, d, g, j) IWP, (b, e, h, k) OD_{liq} , and (c, f, i, l) R_{effliq} retrievals.

through additional information on the horizontal 250 m sub-pixel variability of the MODIS visible reflectance; Zhang *et al.*, 2012). Similarly, DOF filtering on OD_{liq} and R_{effliq} could be lowered by improving our methodology's sensitivity to thin liquid clouds through a better knowledge of the oceanic surface emissivity (e.g. by accounting for wind speed). These modifications are intended for future versions of the ML methodology.

Finally, it is worth noting that such information content analyses can be combined with thorough error analyses in order to gain a more complete understanding of the capabilities of a retrieval method (e.g. Cooper *et al.*, 2007; Sourdeval *et al.*, 2013; Wang *et al.*, 2016a, 2016b).

4. Global retrievals

This section presents global retrievals of the ML methodology for the year 2008. The reader should keep in mind that, as discussed in section 3, the following retrievals correspond to the optimal sensitivity range of our set of measurements (i.e. associated with high partial DOFs and low cost functions), which means that they are only radiatively representative of this range.

4.1. Probability density functions

Figure 7(a)–(c) present the probability density functions (pdfs) associated with retrievals of IWP, OD_{liq} and R_{effliq} , respectively (black lines). The average relative uncertainties attached to each pdf are represented by red lines. The geometric mean and standard deviations of each pdf are indicated in blue above each figure, and the corresponding log-normal distributions are represented by dashed blue lines. Figure 7(a) shows that the IWP retrievals range between about 0.5 and 1000 g m^{-2} , with a geometric mean around 15.25 g m^{-2} . This range clearly emphasises the advantage of combining short-wave and thermal infrared information for retrieving ice cloud properties. The apparent bi-modal distribution seems to be a consequence of different cloud regimes and is in agreement with the pdfs of IWP retrievals obtained from lidar/radar operational products (as will later be shown in section 5.4). The uncertainties attached to ML retrievals vary between more than 100%, for very small and very large IWPs, to about 15–20% between about 15 and 250 g m^{-2} . The small increase in uncertainties around 128 g m^{-2} corresponds to the transition area between retrievals obtained either from the information provided by thermal infrared or from visible channels. Overall, uncertainties better than 25% can be expected between 5 and 500 g m^{-2} . Figure 7(b) shows the pdf of the optical

thickness of the liquid cloud layer. This pdf follows a log-normal-like distribution with a geometric mean around 5.6 and a mode at around 2.5. The associated uncertainties range between 30% for very thin clouds and 10% from an optical thickness of 5. The pdfs associated with the retrievals of the droplet effective radius and their uncertainties are presented in Figure 7(c). Retrievals range between 5 and $30 \mu\text{m}$, with a mode around $12 \mu\text{m}$. Uncertainties on R_{effliq} are of the order of 10%. It can finally be noticed that the fitted log-normal pdfs agree well with the liquid cloud properties.

4.2. Spatial distributions

Global spatial distributions of ML retrievals are presented in Figure 8(a)–(c). Each cloud property is averaged over a $2^\circ \times 2^\circ$ latitude–longitude grid box, using a geometric mean in order to avoid an overestimation of the average due to the log-normal behaviour of their distributions.

The spatial distribution of retrieved IWPs is presented in Figure 8(a). Averaged values between 2 and about 150 g m^{-2} are observed, with a strong dependency upon location. High values of IWP are found in midlatitude storm track regions, in the TWP, and along the ITCZ. Low IWPs, on the contrary, are observed in intertropical subsidence regions, especially over the eastern South Pacific and the South Atlantic Oceans. These results are consistent with recent climatologies of IWP retrievals from passive or active measurements (e.g. Waliser *et al.*, 2009; Eliasson *et al.*, 2011; Li *et al.*, 2012), which nevertheless globally show higher IWP values in the TWP. However, comparisons are difficult because of the use of arithmetic means in most climatologies, which tend to overestimate the averaged grid values. More statistics, covering a longer time period, would also be necessary to validate the distributions observed in Figure 8(a).

Figure 8(b) and (c) show the spatial distribution of OD_{liq} and R_{effliq} , respectively. Averaged values of OD_{liq} around 5 are generally found in open-oceanic intertropical areas, outside of marine stratocumulus regions where they tend to increase. Higher averaged values of OD_{liq} , between 10 and 15, are observed in midlatitude and stratocumulus regions and on the eastern Pacific coasts. Conversely, Figure 8(c) shows low R_{effliq} averaged values (around $10 \mu\text{m}$) in coastal stratocumulus regions and much higher values (above $20 \mu\text{m}$) in open-oceanic intertropical regions. Such high values could nevertheless be the consequence of an overestimation of R_{effliq} for broken clouds with a high sub-pixel horizontal inhomogeneity, as shown by Zhang *et al.* (2012). Figure 6(k) and (l) also show that very low information on OD_{liq}

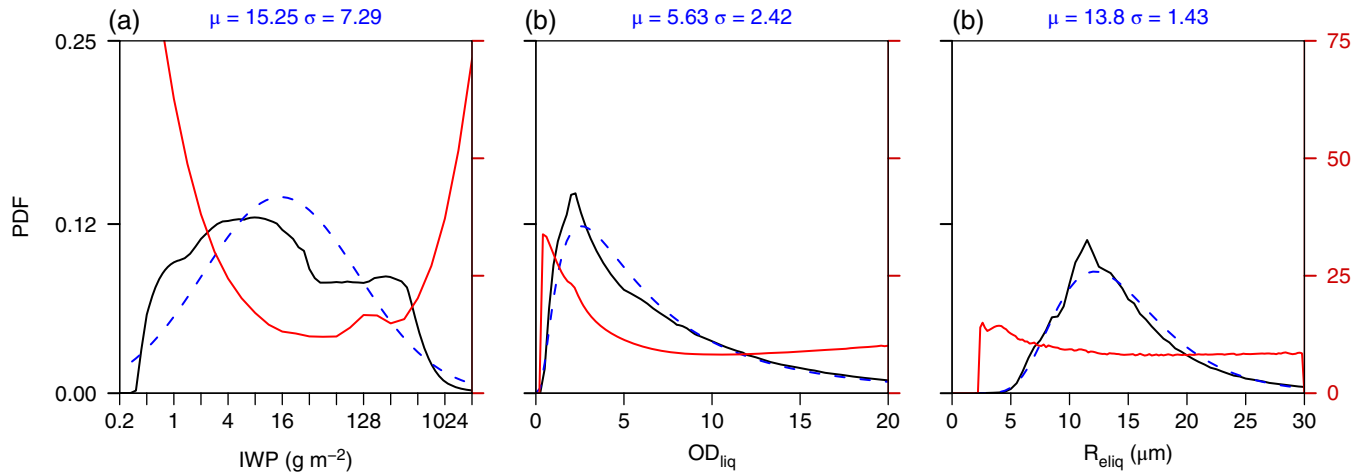


Figure 7. Probability density functions (black lines) corresponding to ML retrievals of (a) IWP, (b) OD_{liq} and (c) $R_{eff,liq}$. The bin-averaged uncertainties associated with the retrievals are indicated by red lines. Dashed blue lines represent the log-normal distributions corresponding to the geometrical mean and standard deviation associated with each retrieved parameter (indicated above each panel in blue).

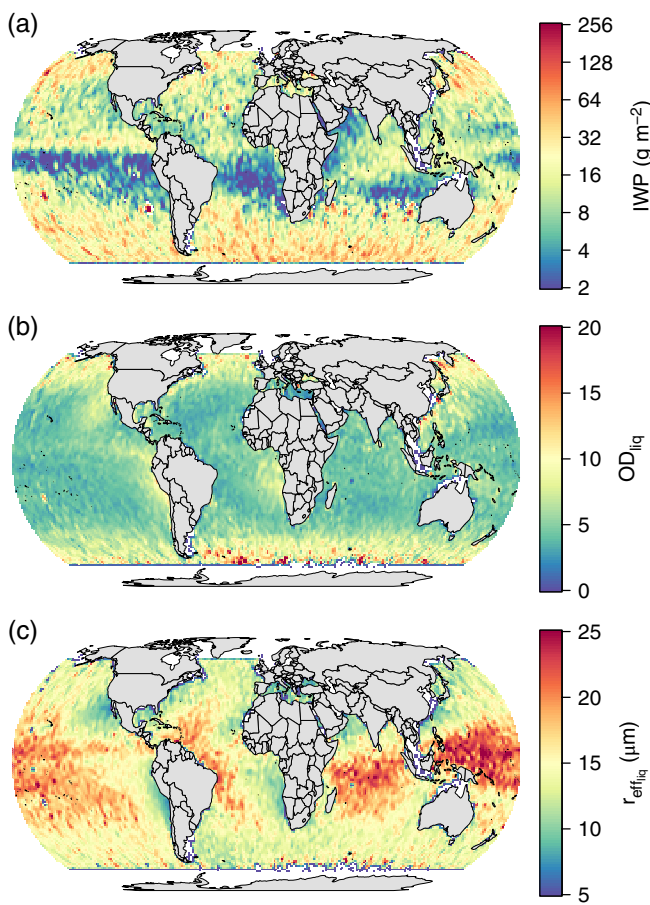


Figure 8. Spatial distribution of ML retrievals of (a) the IWP, (b) the optical thickness of the liquid layer and (c) the droplet effective radius of the liquid layer.

and more particularly $R_{eff,liq}$ is available in these regions, where the cost function and partial DOFs are both high. Overall, these observations are in agreement with those of King *et al.* (2013) from MODIS retrievals, but more statistics are again necessary to confirm these results.

Moreover these spatial dependencies are interesting when coupled to the spatial distribution of types of scene. For instance, it can be observed, when comparing Figures 8(a) and 1(d), that large IWP values are often found in midlatitude regions, where the occurrence of double-layer conditions is relatively high with respect to the total ice cloud fraction. Similarly, Figure 1(c) and (d) show that very few single-layer cases of liquid clouds occur in the TWP and along the ITCZ, where the IWP is also high. Such

observations reaffirm the fact that retrievals and climatologies of liquid cloud properties can strongly be affected by multi-layer conditions if both layers are not properly taken into account.

5. Comparisons to A-Train operational products

This section compares ML retrievals with various operational products from A-Train instruments. Such comparisons aim primarily to validate the results of our method, but can also serve to observe the behaviour of several passive operational products in multi-layer conditions. One-to-one comparisons (i.e. pixel-by-pixel) are presented first, followed by indirect pdf comparisons. These two complementary analyses are required to observe how our retrievals correlate with each operational product and to analyse the overall relevance of ML's pdfs of cloud properties, irrespective of a common sensitivity range. Indeed, the different sensitivity to IWP of each operational algorithm should particularly be kept in mind, as explained in section 5.1.

5.1. Treatment of operational products

Each operational product presented in this section has been colocalized to ML retrievals by finding the smallest coincident distance between them. A minimal distance of 1 km is required in order to include the operational products into the analyses.

Ill-retrieved pixels have been carefully filtered out of each operational product using their respective analysis tools, such as cost function or iteration number in case of retrievals from variational methods or QA flags otherwise. However, no information on the actual sensitivity of operational retrievals to the measurements (e.g. from DOFs) is available.

It should also be kept in mind that the intrinsic range of IWP is much wider than the sensitivity of a single instrument, which means that distributions of IWP retrievals strongly depend on the type(s) of instrument being used. Therefore, only IWPs within the overlapping sensitivity range of both instruments should be utilised when analysing direct comparisons. Considering the log-normal behaviour of the pdfs associated with the products studied here, the range of statistical significance (set as 2σ) for each product x_i is defined as

$$x_i \in [\exp\{\ln(\mu_i) - 2\ln(\sigma_i)\}, \exp\{\ln(\mu_i) + 2\ln(\sigma_i)\}], \quad (3)$$

where μ_i and σ_i are the geometric mean and standard deviation associated with the distribution of x_i , respectively. The subscript ' 2σ ' is later used to indicate that correlation coefficients have been calculated within this range.

Nevertheless it is suspected that, when the two instruments are sensitive to very different IWP ranges, the progressive loss

of information by one instrument and not by the other will produce scatterplots that are not linear at their extremities, but rather curve towards the threshold of complete lack of sensitivity of one instrument. Such areas are particularly difficult to identify *a priori* and risk impacting on the Pearson correlation coefficient $r_{2\sigma}$. However, if the progressive loss of information keeps the scatterplots monotonic, the Spearman correlation coefficient, $\rho_{2\sigma}$, should be able to remain partly unbiased by this phenomenon. This coefficient is indeed very useful to describe how well the relationship between two parameters can be represented by a monotonic function. Its value therefore appears as complementary to $r_{2\sigma}$ in the following analyses.

5.2. Direct comparisons of IWP retrievals

Retrievals of ice cloud properties substantially depend on *a priori* assumptions made on macro- (e.g. geometrical thickness or position of the cloud layer) and micro- (e.g. ice crystal habits, particle size distribution, mass-dimensional relationship) physical properties, which can strongly vary from one retrieval method to another. These assumptions can lead to strong differences between the retrievals if, for instance, ice crystal habits are not consistent with each other (e.g. Dubuisson *et al.*, 2008; Holz *et al.*, 2016). Because their impact is difficult to account for, an expected general agreement within a factor of 2 between ML and each operational product seems reasonable for validation purposes.

5.2.1. Products from active instruments

ML retrievals of IWP are first compared to operational products from active instruments. Since these products provide profiles of cloud properties, the IWP has been calculated by integrating the IWC profile over the whole ice cloud column. Figure 9 shows pixel-by-pixel comparisons between ML (abscissa) and three operational products (ordinate). Comparisons to CALIOP, DARDAR, and 2C-ICE are presented in the first, second, and third rows, respectively. In order to show the capabilities of ML in double-layer situations, the dataset has also been subdivided into three categories. The first column includes IWPs for all the types of scene considered in this study, while the second and third columns isolate retrievals corresponding to single layers of ice clouds and to ice clouds over liquid or mixed-phase cloud layers (hereinafter referred to as double-layer cases), respectively. In each figure, the one-to-one line is shown in black, surrounded by two dashed lines indicating a factor of 2 agreement. The Pearson and Spearman correlation coefficients are also provided.

CALIOP (v3.01) provides lidar-only retrievals of IWP based on an empirical relationship between the IWC and the visible extinction of a cloud layer (Heymsfield *et al.*, 2005). CALIOP is sensitive to optically very thin to moderate ice clouds and its IWC sensitivity range is considered to be between 0.4 and 100 mg m⁻³ (Avery *et al.*, 2012). It is thus expected that CALIOP is more sensitive to small IWPs than our method is, but less sensitive to large IWPs. Figure 9(a) clearly shows the threshold of CALIOP's IWP retrieval from about 30 g m⁻² and highlights the progressive lack of sensitivity of our method below 1 g m⁻². However the latter is not as clear since partial DOFs have been used to filter out such retrievals. Nevertheless comparisons for intermediate IWP values show a good agreement between the two products, well within the factor of 2 area delimited by dashed lines. It can still be observed that CALIOP IWP retrievals are slightly smaller than those of ML. A possible explanation for this behaviour could be that CALIOP is currently known to underestimate IWC retrievals above 12 km due to the facts that its empirical parametrization does not include *in situ* observations from intertropical regions and it is not temperature dependent (Avery *et al.*, 2012). This will be corrected in the upcoming version of CALIOP products (4.0), and therefore subsequent comparisons should help to test this hypothesis. Nevertheless, the observed agreement is already satisfactory for the needs of this study. Finally, it can

be noticed that the Pearson correlation coefficient is low due to the above-mentioned nonlinearities created by the saturation of the lidar signal and the lack of information in our radiometric measurements at the high and low ends of the scatterplots, respectively. However, the Spearman coefficient is less sensitive to these phenomena and shows a correlation of 0.82 between ML and CALIOP. Comparing Figure 9(b) and (c) clearly demonstrates that, despite a lower correlation, ML agrees similarly well with CALIOP in single- and double-layer conditions. It can be noticed in Figure 9(c) that not many retrievals of IWP > 130 g m⁻² appear in double-layer conditions. This is partly due to the current correction that accounts for the vertical inhomogeneity of ice cloud layers, but also to the fact that fewer clouds with high IWP are encountered in such conditions, as later shown in section 5.4.

Comparisons with DARDAR IWP retrievals (v2.1.1 of the CLOUD product) are presented in Figure 9(d). As explained in section 2.1, DARDAR uses the synergy between lidar, radar and radiometric measurements in order to retrieve profiles of ice cloud properties. Its retrievals are based on an optimal estimation scheme, where the IWC corresponds to the integration of an assumed particle mass across a retrieved particle size distribution (PSD; Delanoë *et al.*, 2005; Delanoë and Hogan, 2008, 2010). Thanks to the use of lidar and radar measurements, DARDAR is sensitive to both small and large IWPs. Figure 9(d) shows an agreement within a factor of 2 between ML and DARDAR from about 10 to 250 g m⁻², which includes the area of high frequency of occurrence between about 10 and 60 g m⁻². However the ML methodology seems to progressively underestimate the IWP over 250 g m⁻². This behaviour is explained by progressive saturation of the information provided by the visible channel at such high IWPs. Disagreements are also strong below 10 g m⁻², where ML retrievals are 2–4 times lower than those of DARDAR. However this area is dominated by retrievals obtained in lidar-only conditions (i.e. where the radar is not sensitive), in which DARDAR IWC retrievals are known to be overestimated (Deng *et al.*, 2012). This issue, which impacts IWP retrievals up to about 30 g m⁻², should be improved in the next version of the operational product (Delanoë *et al.*, 2014), but currently makes comparisons between DARDAR and ML difficult for small IWPs. Nevertheless, the Spearman coefficient still indicates a high correlation between the two products. Once again, comparisons between Figure 9(e) and (f) show a similar consistency between ML and DARDAR retrievals in single- and double-layer conditions.

Comparisons to the CloudSat/CALIPSO level-2C ice product (2C-ICE, release 04; Deng *et al.*, 2010) are presented in Figure 9(g). CloudSat 2C-ICE also uses the synergy between lidar and radar information for retrieving profiles of ice cloud properties through an optimal estimation scheme. However the IWC profiles are directly included in the state vector. Figure 9(g) shows that 2C-ICE and ML retrievals agree well within a factor of 2 between 0.5 and 250 g m⁻² and do not display the strong disagreement that was found with DARDAR at small IWPs. This makes 2C-ICE the best reference in the context of our evaluation study. 2C-ICE IWPs are larger than those of ML above about 8 g m⁻² and smaller below. This sharp step seems to correspond to the transition area from lidar-only to lidar-radar retrievals, which could indicate an inconsistency between the parametrizations used to describe ice cloud optical properties for these two instruments. The underestimation of ML retrievals can again be noticed from 250 g m⁻². Nonetheless, ML shows a strong correlation with 2C-ICE retrievals over their common sensitivity ranges, with a Spearman correlation coefficient of 0.93. It can also be noticed that Figure 9(g) shows a higher occurrence of thick clouds with IWP > 130 g m⁻² if compared to Figure 9(d) due to relative differences between IWP distributions of 2C-ICE and DARDAR (as later observed in Figure 13(a)). Finally, comparisons between Figure 9(h) and (i) show that, despite a lesser correlation, retrievals obtained in single- and double-layer conditions are perfectly consistent.

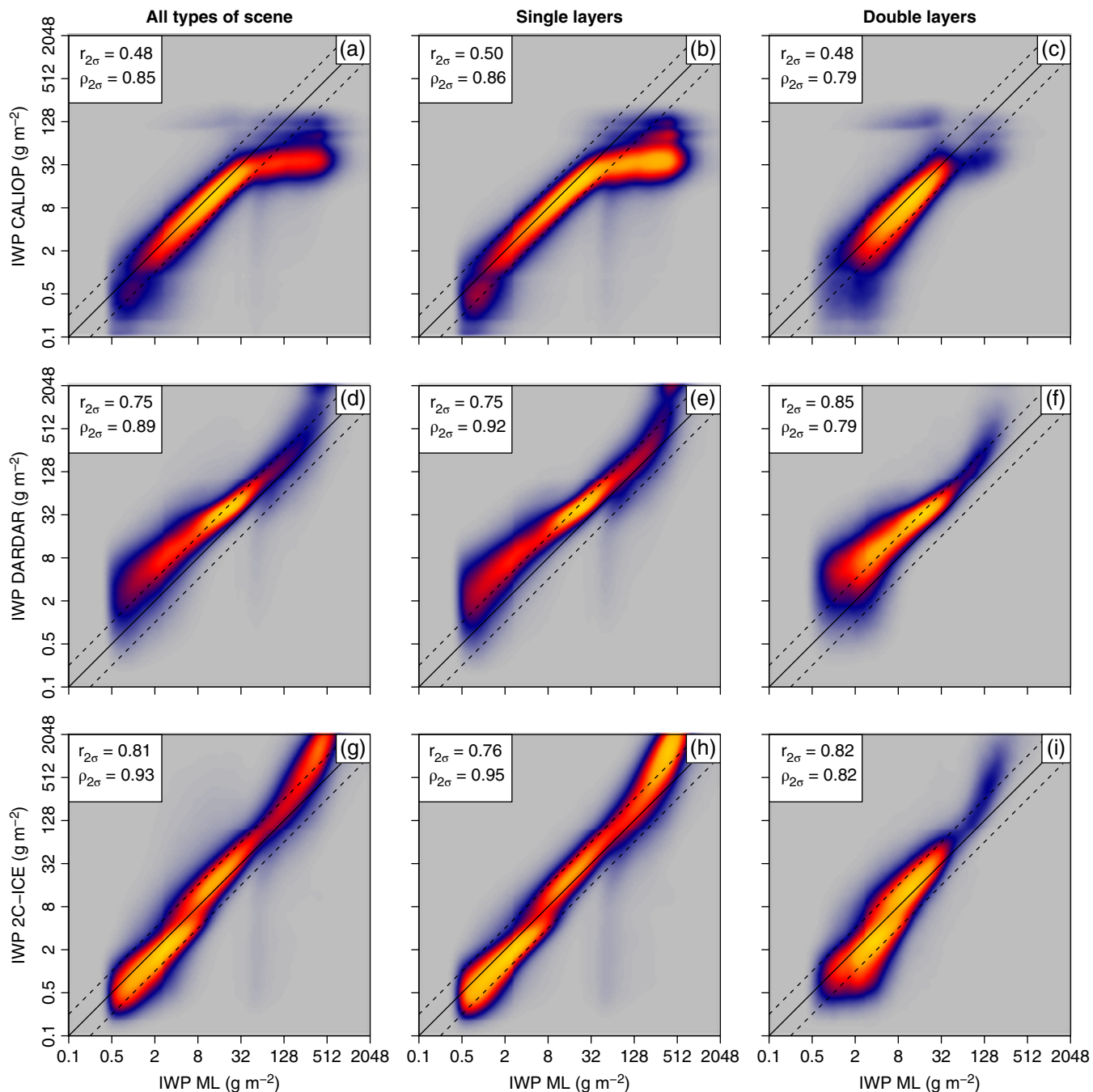


Figure 9. Density scatterplots presenting (a–c) CALIOP, (d–f) DARDAR and (g–i) 2C-ICE IWP retrievals as a function of ML IWP for selected types of scene: (a, d, g) all types of scene, (b, e, h) single ice layers only, and (c, f, i) double ice + As in caption to Figure 1 liquid water/mixed-phase cloud layers only. The plain and dashed black lines indicate the identity line and a factor of 2 around it, respectively. The values of the Pearson $r_{2\sigma}$ and Spearman $\rho_{2\sigma}$ correlation coefficients are obtained from the overlapping area of statistical significance for both products (defined as two standard deviations around the mean).

Figure 9 generally shows that ML retrievals compare well against operational products from active instruments, especially considering that these products also have known above-mentioned issues and that their retrievals do not perfectly agree with each other. Additionally, no particular bias can be observed in ML retrievals obtained in double-layer conditions. It can reasonably be concluded that the observed global agreement between ML and each operational product is a convincing step towards the validation of our IWP retrievals, while keeping in mind that they can be underestimated (but still correlated with radar retrievals) above 250 g m⁻².

5.2.2. Products from passive instruments

Our retrievals are now compared to operational products from passive instruments. Similar to Figures 9, Figure 10(a)–(i) show density scatterplots of ML retrievals against those of IIR (first row), MODIS Collection 5.1 (C5) (second row) and

MODIS Collection 6 (C6) (third row) for several types of scene.

Comparisons to IIR (v3.01) for all types of scene, single-layer only and double-layer only conditions are presented in Figure 10(a)–(c), respectively. IIR calculates the IWP as a direct function of OD and R_e , which are retrieved from the cloud emissivity at 8.5, 10.5, and 12.0 μ m (Garnier *et al.*, 2012, 2013). Despite the fact that IIR only performs single-layer retrievals of ice cloud properties, a second underlying layer can be identified and used as a background reference, which makes the method more robust to the presence of liquid water clouds. Figure 10(a) shows very good agreements between ML and IIR below 130 g m⁻², and a threshold in IIR retrievals above this value due to the saturation of sensitivity in thermal-infrared measurements. Comparing Figure 10(b) and (c) also shows that IIR retrievals do not seem to be significantly impacted by the presence of multi-layer conditions. Despite a better correlation in single-layer case, IIR retrievals remain coherent with those of ML

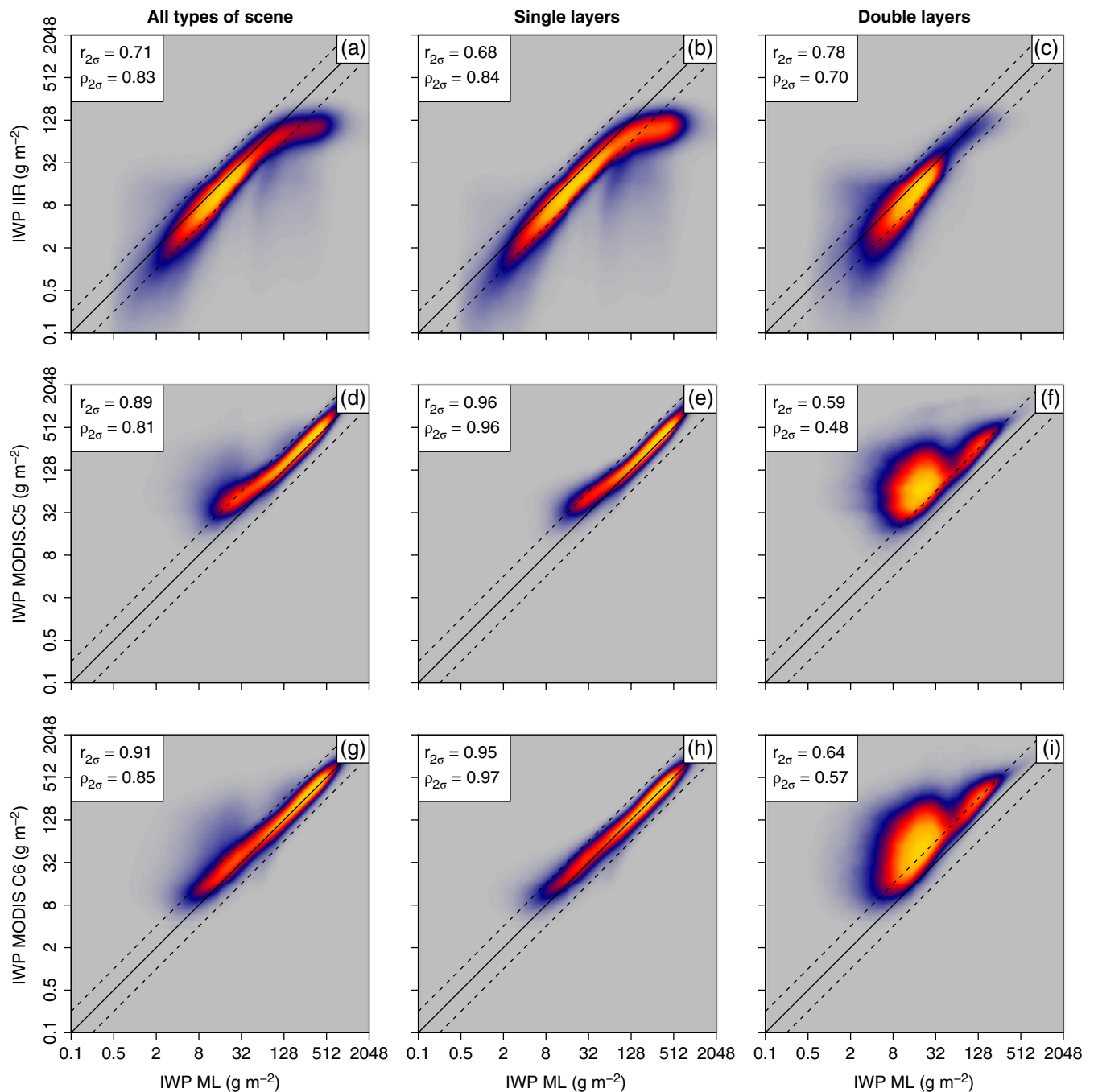


Figure 10. As Figure 9, but presenting (a–c) IIR, (d–f) MODIS C5.1 and (g–i) MODIS C6 retrievals as a function of ML IWP for selected types of scene.

due to their use of an additional opaque liquid cloud layer in the atmospheric column.

Comparisons to MODIS C5 and C6 retrievals are presented in Figure 10(d)–(i). In both versions, MODIS makes use of a couple of visible and near-infrared measurement channels to retrieve the OD and R_e of a cloud layer, which are then directly used for calculating the corresponding IWP (King *et al.*, 1998; Platnick *et al.*, 2014). For consistency, the MODIS IWPs presented in Figure 10(d)–(i) correspond to R_e retrievals obtained from the $2.13\ \mu\text{m}$ channel. Both versions assume a single and vertically homogeneous cloud layer, whose cloud-top altitude and phase (ice or liquid) are provided prior to the retrievals by other MODIS operational products. Several major improvements have been implemented between C5 and C6, among which are an important upgrade of the ice cloud optical properties (e.g. C6 now uses roughened ice crystal habits, similarly to ML) and a re-evaluation of the cloud mask and thermodynamic phase (Marchant *et al.*, 2016). Figure 10(d) shows good general agreement between ML and MODIS C5, but with a strong underestimation of the amount of thin ice clouds in the latter, which does not retrieve IWPs

below $30\ \text{g m}^{-2}$ and very few below $130\ \text{g m}^{-2}$. The agreement is average within this range, with an overestimation of the IWP by MODIS C5, but becomes excellent over $130\ \text{g m}^{-2}$, where both methods use the same visible and near-infrared information. Similar observations can be made concerning single-layer cases presented in Figure 10(e), but with a better correlation between 30 and $130\ \text{g m}^{-2}$. It can be noticed that both correlation coefficients are higher than 0.95. Nevertheless Figure 10(f) shows that, in double-layer conditions, MODIS C5 retrievals are significantly overestimated and less correlated by comparison to those of ML. An explanation for this phenomenon is that, under the single-layer approximation, the reflectance from an underlying liquid cloud layer is mistakenly attributed to the ice cloud, which leads to an overestimation of the integrated ice cloud properties. Such impact of multi-layer conditions on MODIS ice cloud retrievals has for instance already been demonstrated by Chang and Li (2005b) and observed by Davis *et al.* (2009). Further analysis of this phenomenon would require thorough comparisons of MODIS retrievals to products from active instruments, which are however not within the scope of this article as it focuses

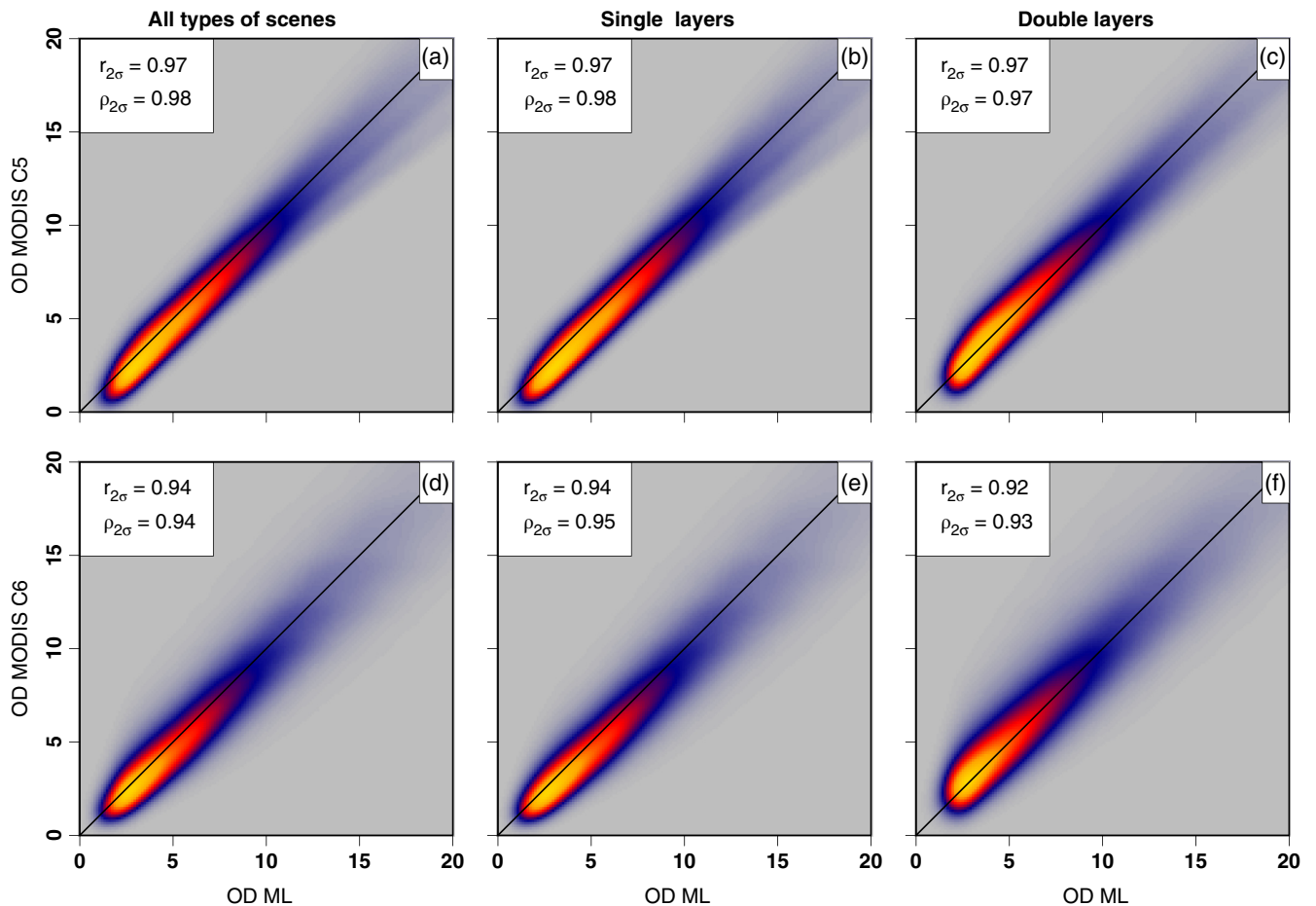


Figure 11. As Figure 9, but presenting (a–c) MODIS C5.1 and (d–f) MODIS C6 retrievals as a function of ML optical depth for selected types of scene: (a, d) all types of scene, (b, e) single liquid water layers only and (c, f) double ice + liquid water cloud only.

on the evaluation of ML products. Comparisons to MODIS C6 show slightly better global agreements with our IWP retrievals, as observed in Figure 10(g) for all types of scene. It can also be noted that MODIS C6 is more sensitive to thinner ice cloud layers than C5, with IWP retrievals down to 10 g m^{-2} . The above-mentioned improvements of the ice cloud microphysics and of the cloud phase discrimination scheme should be responsible for these differences, since no new information is used for the retrievals. Figure 10(h) shows that agreements are again excellent for single ice cloud layer cases, well within a factor of 2 and with correlation coefficients around 0.95. Nonetheless, Figure 10(i) still indicates large differences between ML and MODIS retrievals in double-layer conditions, with comparisons mostly outside the factor 2 area.

Figure 10 therefore shows that ML retrievals are in very good global agreements with each of the operational products, well within a factor of 2 over their respective sensitivity areas. These comparisons also show that ML is capable of IWP retrievals in a much wider range than each operational method taken separately. Finally, a possible impact of multi-layer conditions on MODIS retrievals is observed, but should be confirmed by a more thorough assessment of this phenomenon.

5.3. Direct comparisons of liquid water cloud properties

This section compares ML liquid water cloud retrievals to those of MODIS. MODIS retrieves liquid cloud properties using a similar method to that described in section 5.2.2 for ice clouds. Both ML and MODIS make use of Mie–Lorenz theory for describing the single-scattering properties of cloud droplets and retrieve OD and R_e using the 0.85 and $2.13 \mu\text{m}$ channels, which means that very good agreement is expected.

Figure 11(a)–(f) compare ML OD retrievals with those of MODIS C5 (first row) and C6 (second row). Similar to IWP

comparisons, retrievals from all types of scenes are shown in the first column, while the second and third columns isolate liquid single-layer cases and double-layer cases, respectively. Figure 11(a) shows that excellent agreement is found between ML and MODIS C5, with both correlation coefficients above 0.95. It can be noted that no disagreement between the Pearson and Spearman correlation coefficients is now expected since both methods use the same information. Figure 11(b) and (c) both show extremely good agreements with ML retrievals, which could mean that MODIS C5 OD retrievals should not be strongly biased by the presence of an overlying ice cloud layer. Nevertheless it appears that MODIS OD retrievals are slightly lower than those of ML in the single-layer configuration, while they are in near-perfect agreement in multi-layer conditions. This difference could indicate a small impact of multi-layer conditions on MODIS OD retrievals, as would be expected if the visible reflectance from a cirrus layer were to be mistakenly attributed to the retrieved liquid cloud layer. Moreover it should be kept in mind that MODIS only retrieves the properties of a single cloud layer, whose phase has been identified beforehand. It is thus unlikely that liquid cloud retrievals are provided by MODIS in the presence of an ice cloud which is thick enough to significantly impact the visible measurement channel and subsequently OD retrievals. As a consequence, MODIS liquid cloud retrievals logically appear less impacted by double-layer configurations than ice cloud retrievals are, and it can generally be concluded that MODIS liquid OD retrievals are not statistically too impacted by the presence of an overlying ice cloud layer. Very similar observations can be made regarding comparisons to MODIS C6 retrievals presented in Figure 11(d)–(f), since no major modification on liquid cloud retrievals has been between both versions. However it can be noticed that MODIS C6 and ML OD retrievals are slightly less correlated with each other than previously, particularly in double-layer conditions. Yet, the correlation coefficients remain very high,

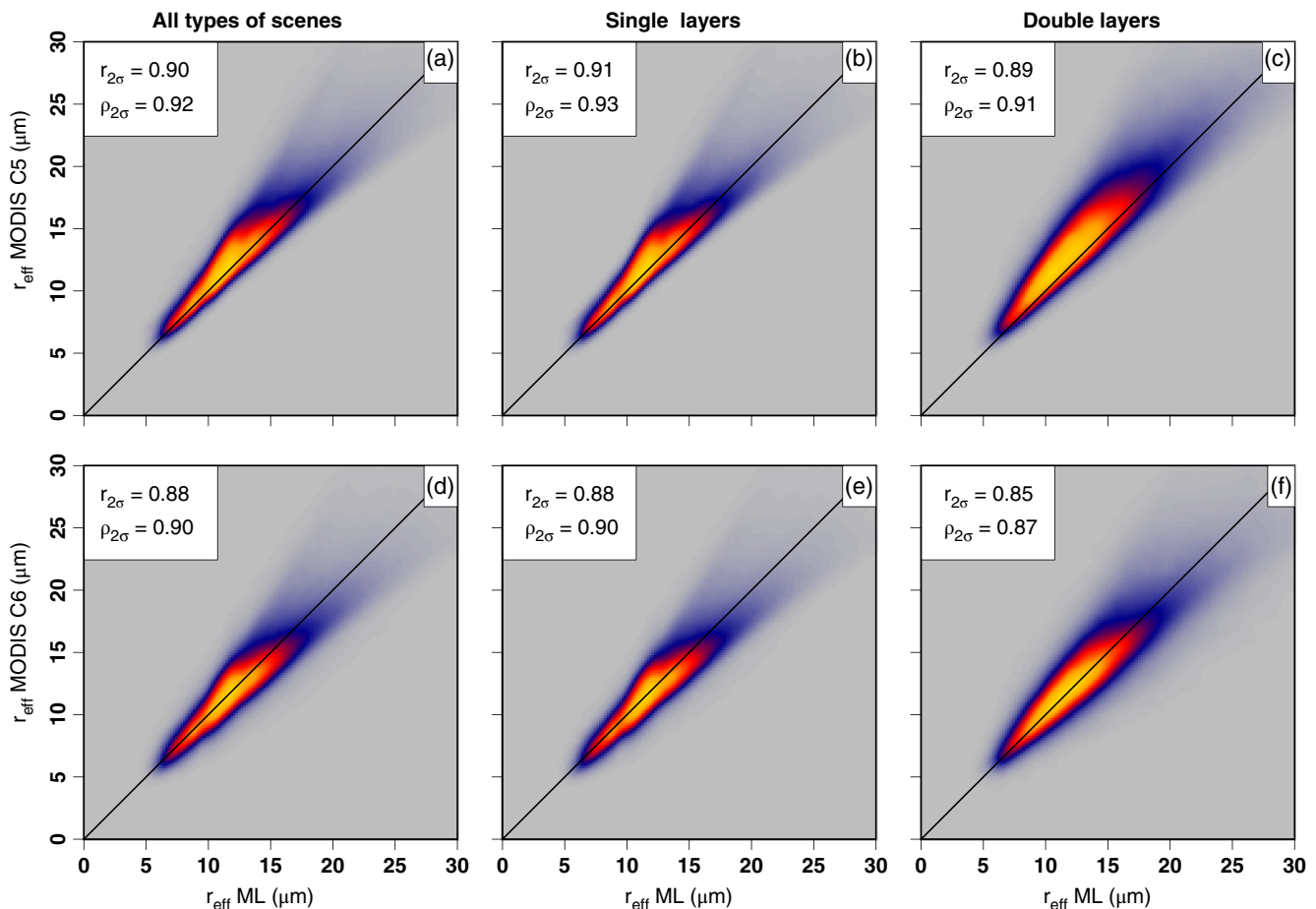


Figure 12. As Figure 11, but for effective radius retrievals.

and it can be concluded that ML OD retrievals compare very well against those of MODIS.

Comparisons of droplet R_e retrievals are similarly presented in Figure 12(a)–(f). Figure 12(a) shows that, for all types of scene, ML and MODIS C5 are in relatively good agreement, with nevertheless slightly larger droplets retrieved by the operational product. Figures 12(b) and (c) indicate that a better agreement is found in single-layer conditions than in the presence of an ice cloud layer, where a bias of about $2\mu\text{m}$ appears. This result is consistent with the fact that near-infrared measurements should be more sensitive to the presence of an ice layer than are visible channels, and therefore that R_e retrievals should more likely be impacted by an ice cloud than the cloud OD. Indeed, in the double-layer configuration, an overestimation of near-infrared reflectances attributed to liquid cloud layers will need to be compensated by the retrieval of larger R_e . Comparisons between ML and MODIS C6, presented in Figure 12(d)–(f), also show good overall agreements, especially in single-layer conditions. However, Figure 12(f) indicates that, for double-layer cases, the overestimation of R_e is much less than for MODIS C5. This behaviour can appear surprising since no direct modification of the way liquid cloud properties are retrieved has been implemented between these versions. However, it can be observed, when comparing Figure 10(d) and (g), that improvements in the ice single-scattering properties and in the phase discrimination process lead C6 to be more sensitive to thinner ice clouds than C5. Hence, it can be understood that MODIS C6 liquid cloud retrievals obtained in multi-layer conditions as associated with the presence of thinner ice cloud layers than in C5. Consequently, optically thick overlying ice clouds are less likely to pollute liquid cloud retrievals in double-layer conditions in C6 than in C5, which explains why the overall overestimation of R_e appears lesser in the latest version of the operational method.

The good general agreement between ML liquid cloud retrievals and MODIS C5 and C6 products observed in Figures 11 and 12 is again a good step towards the validation of our method. However, despite a slight overestimation of R_e in C5, the impact of multi-layer conditions on MODIS products is not obvious from these comparisons and its understanding would therefore require further dedicated analyses.

5.4. Indirect comparisons

The one-to-one comparisons presented in sections 5.2 and 5.3 have the advantage of clearly showing how retrievals directly agree with each other, but do not reflect the coherence of their distribution since they only correspond to the overlapping area of two pdfs. Therefore, in order to complete the previous comparisons, the pdfs of ML retrievals presented in Figure 7 are now compared to those of each aforementioned operational product. Figure 13 shows pdfs of IWP (first column), OD_{liq} (second column), and $R_{e\text{liq}}$ (third column) for all the types of scene considered in this study (first row), single-layer conditions only (second row) and double-layer conditions only (third row). It should be kept in mind that the shapes of these pdfs strongly depend on the type of instrumentation and filtering being used. Perfect agreements are therefore not expected, but these comparisons should serve for observing the overall coherence between ML retrievals and all operational products.

Figure 13(a) presents pdf comparisons of IWP retrievals for ML (back line), IIR (purple), CALIOP (yellow), 2C-ICE (red), DARDAR (green), and MODIS C5 (dashed blue) and C6 (plain blue) for all types of scene. This figure very well illustrates how operational products have a very distinct sensitivity range depending on the type of instrumentation being used. For instance, CALIOP is sensitive to very small IWPs, down to 0.01 g m^{-2} , and its IWP distribution displays a saturation peak around 30 g m^{-2} . IIR is also sensitive to relatively small IWPs,

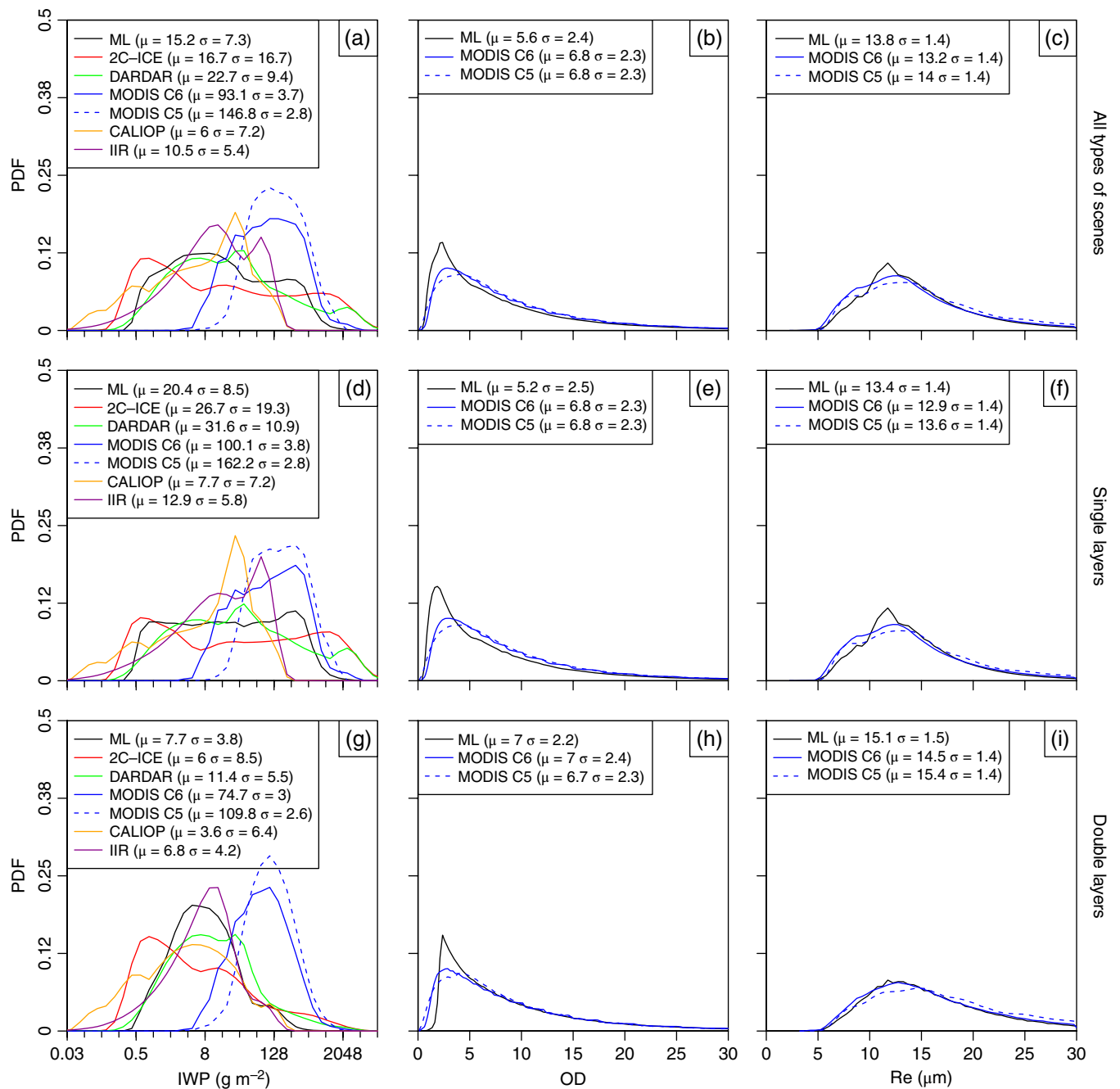


Figure 13. Probability density functions of the (a, d, g) IWP, (b, e, h) optical depth and (c, f, i) droplet effective radius retrieved by several A-Train products in (a–c) all types of scene, (d–f) single-layers only, and (g–i) double-layers only. ML, 2C-ICE, DARDAR, CALIOP and IIR are represented by plain black, red, green, orange and purple lines, respectively. MODIS C5.1 and C6 retrievals are represented by plain and dashed blue lines, respectively. The geometric mean μ and standard deviation σ associated with each retrieval are provided in the legend.

but its infrared measurements tend to lose sensitivity between 60 and 130 g m^{-2} , where a peak also appears. DARDAR and 2C-ICE are both highly sensitive to thin and thick ice clouds, with IWP retrievals ranging from 0.01 to about 8 kg m^{-2} , thanks to the combined use of lidar and radar measurements. Notably, it can be observed that the geometric mean of ML retrievals is coherent with that of these two products, with 15.2 g m^{-2} for ML against 16.7 and 22.7 g m^{-2} for 2C-ICE and DARDAR, respectively. As expected, their geometric standard deviations are nevertheless larger, with 7.3 g m^{-2} for ML against 16.7 and 9.4 g m^{-2} for 2C-ICE and DARDAR, respectively. The pdfs associated with MODIS retrievals logically display a shifted sensitivity towards thick ice clouds due to the use of visible and near-infrared measurements alone, with geometric means of 93.1 and 146.8 g m^{-2} for C6 and C5, respectively. However it is clear that the upgrades performed in C6 allow a better sensitivity to thin ice clouds, with IWPs down to 4 g m^{-2} . These limits should nevertheless be treated carefully since no operational products have been filtered to

narrow their pdfs to the optimal sensitivity of the retrieval method. Nonetheless, Figure 13(a) again demonstrates the advantage of merging visible and thermal infrared measurements in order to widen the sensitivity of IWP retrieval methods. Figure 13(d) shows that larger values of IWP are generally found in single-layer cases, with a clear shift of each distribution in that direction. Higher saturation peaks also appear for methods that are less sensitive to thick ice clouds, such as IIR and CALIOP. Besides, a clear peak appears in ML retrievals and shows the limitation of the retrieval method from IWPs between about 250 and 500 g m^{-2} . These values logically correspond to the maximum sensitivity area of MODIS C5 and C6, which use the same information in this IWP range. One can note that the geometric mean from ML retrievals is again very similar to that of 2C-ICE and DARDAR, around 25 g m^{-2} . In double-layer conditions, Figure 13(g) shows that the pdfs are on the contrary shifted towards small IWP values, with geometric means of 6.0 and 11.4 g m^{-2} for 2C-ICE and DARDAR, respectively. ML and IIR are perfectly able to follow

this tendency, with means around 7.7 and 6.8 g m⁻², respectively, while MODIS retrievals remain very high. This also shows that MODIS is only sensitive to a small portion of ice clouds in double-layer conditions. Moreover, these comparisons to DARDAR and 2C-ICE show that very high IWP values are not very occurrent in multi-layer conditions and therefore that the lack of information in the current version of ML to retrieve high IWPs in multi-layer conditions should not be too critical.

Figure 13(b) presents pdfs of liquid cloud OD retrievals for ML and MODIS C6 and C5. As expected, these pdfs are very similar to each other but one can still notice a higher frequency of small ODs in our method. The geometric mean corresponding to ML retrievals is 5.6 against 6.8 for both MODIS versions. Nevertheless the spread is similar between the retrieval methods. The same observation can also be made in single-layer conditions, as shown in Figure 13(e), and is therefore difficult to explain due to the use of identical measurements and similar single-scattering properties for describing the cloud droplet in both methods. Possible explanations could be related to a different treatment of gaseous absorption, scattering phenomena in radiative transfer calculations, or the use of look-up tables for MODIS retrievals, and will require further investigations. Nevertheless the observed agreement is satisfactory for our current evaluation purposes. In double-layer conditions, Figure 13(h) shows a strong decrease of OD retrievals in ML below values of about 2. This is explained by the lack of information on small ODs in the presence of an ice cloud layer, which generally leads to a stronger filtering due to lower partial DOF values, in agreement with Figure 4(b). The MODIS pdfs do not seem affected by the presence of an ice cloud layer, as their geometric mean and standard deviation remain identical to those obtained in single-layer conditions, but it should be kept in mind that these retrievals of liquid cloud OD are only obtained in the presence of thin ice clouds, which should therefore not strongly impact the visible measurements.

Figure 13(c) shows good agreement between the pdfs of R_{cliq} for ML and MODIS. The geometric means corresponding to these distributions are 13.8, 13.2, and 14 μm for ML, MODIS C5 and C6, respectively, with a geometric standard deviation of 1.4 μm for each distribution. Nevertheless it can be observed that ML has a lower occurrence of small droplets, which can also be a consequence of the partial DOF filtering. It has indeed been seen in Figure 5 that R_{cliq} is very sensitive to this type of filtering due to a strong lack of sensitivity on this parameter in the case of optically thin liquid clouds or the presence of optically thick ice clouds, as displayed in Figure 4(c). Small values of R_{cliq} should be particularly affected by this filtering and such values consequently occur less in the pdf. Identical observations can be made in single and multi-layer conditions, as shown in Figure 13(f) and (i), respectively. One can notice in the latter case that each retrieval method obtains high values of R_{cliq} , with a mean around 15 μm , which leads to better overall agreements of the pdfs.

6. Summary and conclusions

This article has presented one year of near-global multi-layer retrievals of ice and liquid cloud properties obtained from the ML methodology in daytime conditions, over an oceanic surface, and excluding high-latitude regions. The methodology has the strong advantage that it can simultaneously retrieve integrated properties of ice and liquid water clouds, thanks to the use of radiometric measurements ranging from the visible to the thermal infrared. This particular set of channels additionally allows sensitivity to optically thick and thin ice clouds. The capabilities and limitations of this method have been demonstrated theoretically and illustrated briefly in the first part of this study; here they have been globally analysed and thoroughly evaluated against five A-Train operational products.

However a few elements from the original methodology have been updated to better fit the needs of an application to global measurements. These include the use of a lidar/radar product,

for positioning and discriminating the phase of cloud layers, and an additional uncertainty on the vertical inhomogeneity and top altitude of ice cloud layers. The last two were necessary to properly retrieve the IWP of thick ice cloud layers, where the vertical homogeneity assumption is no longer realistic.

This study has first illustrated how analysis tools provided by the ML methodology can be utilised for a thorough filtering of the dataset: the cost function removes retrievals that do not allow the forward model to converge towards the measurements, and partial DOFs eliminate any strong dependency on *a priori* assumptions. A few types of scene containing mixed-phase clouds have also been removed from the analyses. Consequently, about 30% of IWP retrievals and 45 and 75% of liquid cloud OD and R_e retrievals, respectively, have been rejected by this filtering process. These numbers clearly illustrate the importance of using such analysis tools for properly analysing retrievals and therefore constraining the existing uncertainties on cloud properties.

An analysis of pdfs associated with the selected retrievals has shown that our methodology is capable of retrieving a wide range of IWPs, from about 0.5 to 1000 g m⁻², with uncertainties better than 25% between 5 and 500 g m⁻². This observation clearly demonstrates the strong advantage of merging visible and thermal infrared measurements for ice cloud retrievals. Uncertainties on the liquid cloud OD vary from 30% for very thin clouds to about 10% from an OD of 4. The retrievals of droplet R_e are usually associated with uncertainties of 10%. Moreover, joint analyses of the spatial distribution of these retrievals with the occurrence of multi-layer conditions remind us of the importance of properly treating multi-layer conditions in order not to bias global climatologies, as both strongly depend upon location.

ML IWP retrievals have directly been compared to five active and passive operational products from the A-Train: IIR, MODIS (C5 and C6), CALIOP, DARDAR, and 2C-ICE. We observed that ML IWP retrievals agree well within a factor of 2 with every active product over their respective sensitivity range. Nevertheless it appeared that ML can progressively underestimate the IWP from 250 g m⁻² due to a saturation of the information provided by the visible channel. We have found very good agreements with products from passive measurements in single-layer conditions. It was also noted that retrieval methods under the single-layer approximation can be significantly affected by the presence of a liquid cloud layer, which leads to a strong overestimation of the IWP. We found extremely good agreement when comparing OD and droplet R_e retrievals to those of MODIS C5 and C6 in single-layer conditions. Despite a slight overestimation of R_e by MODIS C5 in multi-layer conditions, no strong impact from the presence of ice cloud layers was noticed in MODIS liquid cloud retrievals. However, it should be kept in mind that these retrievals are mainly obtained in the presence of very thin ice cloud layers which are unlikely to significantly impact liquid cloud properties. Further analyses and comparisons are therefore necessary for a thorough assessment of the impact of multi-layer conditions on existing A-Train products.

This study also found good agreements when indirectly comparing each operational product to the pdfs of ML retrievals. It was observed that the pdfs of ML liquid cloud OD and droplet R_e retrievals are very similar to those of MODIS, despite a higher occurrence of small ODs in our method, which should further be investigated. The pdfs of ML IWP retrievals are also perfectly coherent with most operational products, in particular DARDAR and 2C-ICE. In spite of a narrower spread, our retrievals have been found to globally follow the distribution of these two lidar/radar methods and provide very similar geometric means in single and double-layer conditions.

We therefore conclude that these agreements between ML and A-Train operational products lead to a very strong step towards the validation of the results of our retrieval method. Future work will include a deeper analysis of the results of the dataset for

several years of retrievals and a more thorough assessment of the impact of the single-layer assumption on existing retrievals and climatologies.

Future improvements of the methodology will focus on the inclusion of additional measurements in the state vector for retrieving a cloud-top altitude in order to stray from the lidar track. Lidar and radar measurements will nevertheless remain to serve as *a priori* information for these retrievals. A proper treatment of the vertical inhomogeneity of the ice cloud layer is also necessary in order to improve the quality of retrievals in the presence of thick ice clouds.

Finally, it should be noted that the ML methodology is perfectly adequate in the frame of the future EarthCare mission, which will include a Multi-Spectral Imager (MSI) with channels adapted to our measurement vector (0.67, 0.86, 1.67, 2.21, 8.8, 10.8 and $12.0\mu\text{m}$) (Illingworth *et al.*, 2015). The ATmospheric LIDar (ATLID) and a Cloud Profiling Radar (CPR), included on the same platform, are also adapted to provide *a priori* information on the position of cloud layers.

Acknowledgements

This work was funded by the Federal Ministry of Education and Research in Germany (BMBF) through the research programme ‘High Definition Clouds and Precipitation for Climate Prediction –HD(CP)2’ (FKZ: 01LK1210D) and the Centre National d’Études Spatiales (CNES). We want to acknowledge the ICARE data centre (<http://www.icare.univ-lille1.fr>; accessed 14 Aug 2016) for providing the A-Train data used in this study, and J. Delanoë for the access to the DARDAR products. We are grateful to the Laboratoire d’Optique Atmosphérique (LOA) and the Deutsches Klimarechenzentrum (DKRZ) for providing computational resources necessary for this study.

Appendix

Inferring the ice cloud optical depth in ML

A detailed description of the ice cloud properties used in ML can be found in section 3.2.5 of S15, but some aspects are partly repeated here due to the novelty of such parametrization in passive remote sensing retrievals.

The single-scattering properties (i.e. mass extinction coefficient σ_{ext} , single-scattering albedo ω_0 , and asymmetry parameter g) used in ML are provided by a parametrization by Baran *et al.* (2014), which expresses these properties as function of IWC and temperature T_c in an ice cloud layer. This is a

direct consequence of the integration of the ensemble model by Baran and Labonnote (2007), which provides the single-scattering properties of roughened ice crystal habits as a function of their size, over particle size distributions (PSD) provided by a single-moment bulk snow parametrization (Field *et al.*, 2007). The latter is based on a PSD rescaling method (e.g. Lee *et al.*, 2004; Testud *et al.*, 2001) which was applied to a large number of midlatitude and tropical *in situ* measurements, and provides an estimation of any moment of an ice crystal PSD based on the second moment (related to the IWC) and the temperature. The necessity for a temperature dependency reflects a relationship between T_c and the ice crystal size and number concentration due to aggregation processes. Therefore, for a given IWC and T_c , a realistic ice crystal PSD can be estimated and used to integrate the mixture of ice crystals from the ensemble model, which in turn provides the single-scattering properties. As a consequence, only the IWC (or the IWP, assuming vertical homogeneity) together with a temperature profile (here provided by reanalyses) are necessary to perform forward model simulations and retrievals. Nevertheless, the optical depth OD_{ice} can still be inferred from our IWP retrievals, as explained below. It can also be noted that similar parametrizations are already used in operational active remote sensing products (e.g. Delanoë *et al.*, 2005, 2014; Hogan *et al.*, 2006, for DARDAR).

In ML, each ice cloud layer is vertically described by 100 m sub-layers that are characterised by an IWC (inferred from the IWP) and a temperature. Subsequently, the Baran *et al.* (2014) parametrization is used to associate single-scattering properties to each sub-layer, and the obtained σ_{ext} profile can be vertically integrated over the cloud depth in order to infer OD_{ice} . Figure A1 shows an example of visible OD_{ice} retrievals from ML, compared to those of 2C-ICE and MODIS C6. More details on these datasets can be found in section 5. These two products are chosen here as they represent in this study the best references for active and passive remote sensing retrievals, respectively. For reasons of clarity, only retrievals obtained in single-layer conditions are shown in this Appendix. It can be observed that, similar to comparisons presented in section 5, very good agreements are found between ML and both products. Comparisons to 2C-ICE show that ML agrees well within a factor of 2 with this active product, from very small to very large optical depths. The correlation is also very high with MODIS C6 from moderate to high OD_{ice} values, despite a small bias that could be due to differences of ice crystal habits used in the retrievals (e.g. Holz *et al.*, 2016). This clearly demonstrates the ability of ML to infer an ice cloud optical depth from its IWP retrievals and a corresponding T_c profile.

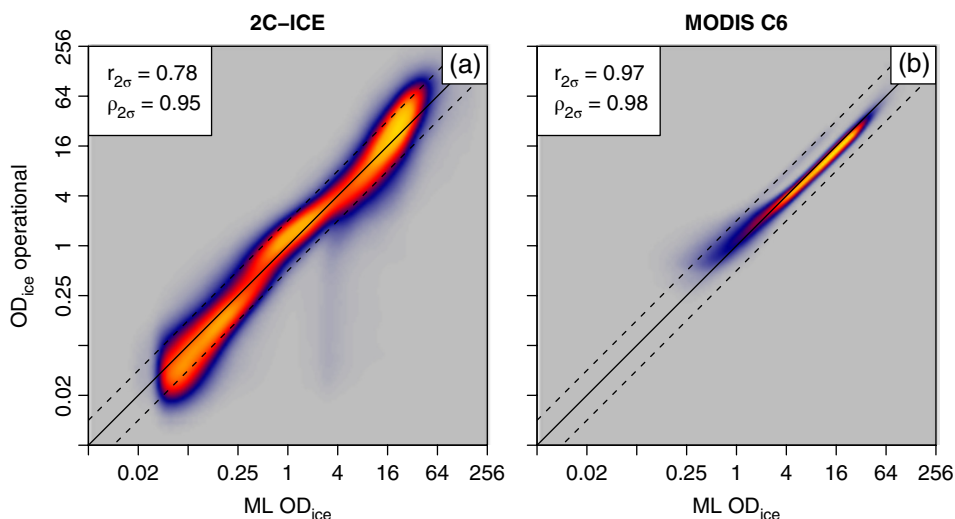


Figure A1. As Figure 10, but showing scatterplot of (a) 2C-ICE and (b) MODIS C6 visible ice cloud optical depth (OD_{ice}) as a function of ML OD_{ice} , for single-layer ice cloud layers.

References

- Austin RT, Heymsfield AJ, Stephens GL. 2009. Retrieval of ice cloud microphysical parameters using the CloudSat millimeter-wave radar and temperature. *J. Geophys. Res.: Atmos.* **114**: D00A23, doi: 10.1029/2008JD010049.
- Avery M, Winker DM, Heymsfield AJ, Vaughan M, Young SA, Hu Y, Trepte C. 2012. Cloud ice water content retrieved from the CALIOP space-based lidar. *Geophys. Res. Lett.* **39**: L05808, doi: 10.1029/2011GL050545.
- Baran AJ. 2012. From the single-scattering properties of ice crystals to climate prediction: A way forward. *Atmos. Res.* **112**: 45–69, doi: 10.1016/j.atmosres.2012.04.010.
- Baran AJ, Labonnote L. 2007. A self-consistent scattering model for cirrus. I: The solar region. *Q. J. R. Meteorol. Soc.* **133**: 1899–1912.
- Baran AJ, Cotton R, Furtado K, Havemann S, Labonnote LC, Marengo F, Smith A, Thelen JC. 2014. A self-consistent scattering model for cirrus. II: The high and low frequencies. *Q. J. R. Meteorol. Soc.* **140**: 1039–1057, doi: 10.1002/qj.2193.
- Brenguier JL, Pawlowska H, Schüller L, Preusker R, Fischer J, Fouquart Y. 2000. Radiative properties of boundary-layer clouds: Droplet effective radius versus number concentration. *J. Atmos. Sci.* **57**: 803–821, doi: 10.1175/1520-0469(2000)057<0803:RPOBLC>2.0.CO;2.
- Ceccaldi M, Delanoë J, Hogan RJ, Pounder NL, Protat A, Pelon J. 2013. From CloudSat-CALIPSO to Earthcare: Evolution of the DARDAR cloud classification and its comparison to airborne radar–lidar observations. *J. Geophys. Res.: Atmos.* **118**: 7962–7981, doi: 10.1002/jgrd.50579.
- Chang FL, Li Z. 2005a. A near-global climatology of single-layer and overlapped clouds and their optical properties retrieved from TERRA/MODIS data using a new algorithm. *J. Clim.* **18**: 4752–4771, doi: 10.1175/JCLI3553.1.
- Chang FL, Li Z. 2005b. A new method for detection of cirrus overlapping water clouds and determination of their optical properties. *J. Atmos. Sci.* **62**: 3993–4009, doi: 10.1175/JAS3578.1.
- Cho HM, Zhang Z, Meyer K, Lebsock M, Platnick S, Ackerman AS, Di Girolamo L, C-Labonnote L, Cornet C, Riedi J, Holz RE. 2015. Frequency and causes of failed MODIS cloud property retrievals for liquid phase clouds over global oceans. *J. Geophys. Res.: Atmos.* **120**: 4132–4154, doi: 10.1002/2015JD023161.
- Cooper SJ, L'Ecuyer TS, Gabriel P. 2006. Objective assessment of the information content of visible and infrared radiance measurements for cloud microphysical property retrievals over the global oceans. Part II: Ice clouds. *J. Appl. Meteorol.* **45**: 42–62.
- Cooper SJ, L'Ecuyer TS, Gabriel P, Baran AJ. 2007. Performance assessment of a five-channel estimation-based ice cloud retrieval scheme for use over the global oceans. *J. Geophys. Res.* **112**: D04207, doi: 10.1029/2006JD007122.
- Davis SM, Avallone LM, Kahn BH, Meyer KG, Baumgardner D. 2009. Comparison of airborne *in situ* measurements and moderate resolution imaging spectroradiometer (MODIS) retrievals of cirrus cloud optical and microphysical properties during the midlatitude cirrus experiment (MIDCIX). *J. Geophys. Res.: Atmos.* **114**: D02203, doi: 10.1029/2008JD010284.
- Delanoë J, Hogan RJ. 2008. A variational scheme for retrieving ice cloud properties from combined radar, lidar, and infrared radiometer. *J. Geophys. Res.* **113**: D07204, doi: 10.1029/2007JD009000.
- Delanoë J, Hogan RJ. 2010. Combined CloudSat-CALIPSO-MODIS retrievals of the properties of ice clouds. *J. Geophys. Res.* **115**: D00H29, doi: 10.1029/2009JD012346.
- Delanoë J, Protat A, Testud J, Bouniol D, Heymsfield AJ, Bansemmer A, Brown PRA, Forbes RM. 2005. Statistical properties of the normalized ice particle size distribution. *J. Geophys. Res.* **110**: D10201, doi: 10.1029/2004JD005405.
- Delanoë J, Heymsfield AJ, Protat A, Bansemmer A, Hogan RJ. 2014. Normalized particle size distribution for remote sensing application. *J. Geophys. Res.: Atmos.* **119**: 4204–4227, doi: 10.1002/2013JD020700.
- Deng M, Mace GG, Wang Z, Okamoto H. 2010. Tropical composition, cloud and climate coupling experiment validation for cirrus cloud profiling retrieval using CloudSat radar and CALIPSO lidar. *J. Geophys. Res.: Atmos.* **115**: D00J15, doi: 10.1029/2009JD013104.
- Deng M, Mace GG, Wang Z, Lawson RP. 2012. Evaluation of several a-train ice cloud retrieval products with *in situ* measurements collected during the sparticus campaign. *J. Appl. Meteorol. Climatol.* **52**: 1014–1030, doi: 10.1175/JAMC-D-12-054.1.
- Dubuisson P, Giraud V, Pelon J, Cadet B, Yang P. 2008. Sensitivity of thermal infrared radiation at the top of the atmosphere and the surface to ice cloud microphysics. *J. Appl. Meteorol. Climatol.* **47**: 2545–2560.
- Eliasson S, Buehler SA, Milz M, Eriksson P, John VO. 2011. Assessing observed and modelled spatial distributions of ice water path using satellite data. *Atmos. Chem. Phys.* **11**: 375–391, doi: 10.5194/acp-11-375-2011.
- Fauchez T, Dubuisson P, Cornet C, Szczap F, Garnier A, Pelon J, Meyer K. 2015. Impacts of cloud heterogeneities on cirrus optical properties retrieved from space-based thermal infrared radiometry. *Atmos. Meas. Tech.* **8**: 633–647, doi: 10.5194/amt-8-633-2015.
- Feofilov AG, Stubenrauch CJ, Delanoë J. 2015. Ice water content vertical profiles of high-level clouds: Classification and impact on radiative fluxes. *Atmos. Chem. Phys. Discuss.* **15**: 16325–16369, doi: 10.5194/acpd-15-16325-2015.
- Field PR, Heymsfield A, Bansemmer A. 2007. Snow size distribution parameterization for midlatitude and tropical ice clouds. *J. Atmos. Sci.* **64**: 4346–4365, doi: 10.1175/2007JAS2344.
- Garnier A, Pelon J, Dubuisson P, Faivre M, Chomette O, Pascal N, Kratz DP. 2012. Retrieval of cloud properties using CALIPSO imaging infrared radiometer. Part I: Effective emissivity and optical depth. *J. Appl. Meteorol. Climatol.* **51**: 1407–1425, doi: 10.1175/JAMC-D-11-0220.1.
- Garnier A, Pelon J, Dubuisson P, Yang P, Faivre M, Chomette O, Pascal N, Lucker P, Murray T. 2013. Retrieval of cloud properties using CALIPSO imaging infrared radiometer. Part II: Effective diameter and ice water path. *J. Appl. Meteorol. Climatol.* **52**: 2582–2599, doi: 10.1175/JAMC-D-12-0328.1.
- Ham SH, Sohn BJ, Kato S, Satoh M. 2013. Vertical structure of ice cloud layers from CloudSat and CALIPSO measurements and comparison to NICAM simulations. *J. Geophys. Res.: Atmos.* **118**: 9930–9947, doi: 10.1002/jgrd.50582.
- Heidinger AK, Pavlonis MJ. 2005. Global daytime distribution of overlapping cirrus cloud from NOAA's Advanced Very High Resolution Radiometer. *J. Clim.* **18**: 4772–4784, doi: 10.1175/JCLI3535.1.
- Heymsfield AJ, Winker D, van Zadelhoff GJ. 2005. Extinction-ice water content-effective radius algorithms for CALIPSO. *Geophys. Res. Lett.* **32**: L10807, doi: 10.1029/2005GL022742.
- Hogan RJ, Mittermaier MP, Illingworth AJ. 2006. The retrieval of ice water content from radar reflectivity factor and temperature and its use in evaluating a mesoscale model. *J. Appl. Meteorol. Climatol.* **45**: 301–317, doi: 10.1175/JAM2340.1.
- Holz RE, Platnick S, Meyer K, Vaughan M, Heidinger A, Yang P, Wind G, Dutcher S, Ackerman S, Amarasinghe N, Nagle F, Wang C. 2016. Resolving ice cloud optical thickness biases between CALIOP and MODIS using infrared retrievals. *Atmos. Chem. Phys.* **16**: 5075–5090, doi: 10.5194/acp-16-5075-2016.
- Hu Y, Winker D, Vaughan M, Lin B, Omar A, Trepte C, Flittner D, Yang P, Nasiri SL, Baum B, Holz R, Sun W, Liu Z, Wang Z, Young S, Stamnes K, Huang J, Kuehn R. 2009. CALIPSO/CALIOP cloud phase discrimination algorithm. *J. Atmos. Oceanic Technol.* **26**: 2293–2309, doi: 10.1175/2009JTECHA1280.1.
- Illingworth AJ, Barker HW, Beljaars A, Ceccaldi M, Chepfer H, Clerbaux N, Cole J, Delanoë J, Domenech C, Donovan DP, Fukuda S, Hirakata M, Hogan RJ, Huenerbein A, Kollias P, Kubota T, Nakajima T, Nakajima TY, Nishizawa T, Ohno Y, Okamoto H, Oki R, Sato K, Satoh M, Shephard MW, Velázquez-Blázquez A, Wandinger U, Wehr T, van Zadelhoff GJ. 2015. The Earthcare satellite: The next step forward in global measurements of clouds, aerosols, precipitation, and radiation. *Bull. Am. Meteorol. Soc.* **96**: 1311–1332, doi: 10.1175/BAMS-D-12-00227.1.
- Inoue T. 1985. On the temperature and effective emissivity determination of semi-transparent cirrus clouds by bi-spectral measurements in the 10 μ m window region. *J. Meteorol. Soc. Jpn.* **63**: 88–98.
- IPCC. 2013. *Climate Change 2013: The Physical Science Basis. Contribution of Working Group I to the Fifth Assessment Report of the Intergovernmental Panel on Climate Change*. Cambridge University Press: Cambridge, UK and New York, NY, doi: 10.1017/CBO9781107415324.
- Joiner J, Vasilkov AP, Bhartia PK, Wind G, Platnick S, Menzel WP. 2010. Detection of multi-layer and vertically extended clouds using A-train sensors. *Atmos. Meas. Tech.* **3**: 233–247, doi: 10.5194/amt-3-233-2010.
- King MD, Tsay SC, Platnick S, Wang M, Liou KN. 1998. *Cloud Retrieval Algorithms for MODIS: Optical Thickness, Effective Particle Radius, and Thermodynamic Phase*, Algorithm Theoretical Basis Document ATBD-MOD-05. NASA Goddard Space Flight Center: Greenbelt, MD.
- King MD, Platnick S, Menzel WP, Ackerman SA, Hubanks PA. 2013. Spatial and temporal distribution of clouds observed by MODIS onboard the Terra and Aqua satellites. *IEEE Trans. Geosci. Remote Sens.* **51**: 3826–3852.
- L'Ecuyer TS, Gabriel P, Leesman K, Cooper SJ, Stephens GL. 2006. Objective assessment of the information content of visible and infrared radiance measurements for cloud microphysical property retrievals over the global oceans. Part I: Liquid clouds. *J. Appl. Meteorol. Climatol.* **45**: 20–41, doi: 10.1175/JAM2326.1.
- Lee GW, Zawadzki I, Szyrmer W, Sempere-Torres D, Uijlenhoet R. 2004. A general approach to double-moment normalization of drop size distributions. *J. Appl. Meteorol.* **43**: 264–281, doi: 10.1175/1520-0450(2004)043<0264:AGATDN>2.0.CO;2.
- Li JLF, Waliser DE, Chen WT, Guan B, Kubar T, Stephens G, Ma HY, Deng M, Donner L, Seman C, Horowitz L. 2012. An observationally based evaluation of cloud ice water in CMIP3 and CMIP5 GCMs and contemporary reanalyses using contemporary satellite data. *J. Geophys. Res.: Atmos.* **117**: D16105, doi: 10.1029/2012JD017640.
- Liu Z, Omar AH, Hu Y, Vaughan MA, Winker DM. 2005. *CALIOP Algorithm Theoretical Basis Document—Part 3: Scene Classification Algorithms*, Doc. pc-sci-202 part 3. NASA Langley Research Center: Hampton, VA.
- Marchant B, Platnick S, Meyer K, Arnold GT, Riedi J. 2016. MODIS collection 6 shortwave-derived cloud phase classification algorithm and comparisons with CALIOP. *Atmos. Meas. Tech.* **9**: 1587–1599, doi: 10.5194/amt-9-1587-2016.
- Marks CJ, Rodgers CD. 1993. A retrieval method for atmospheric composition from limb emission measurements. *J. Geophys. Res.* **98**: 14939–14953, doi: 10.1029/93JD01195.
- Mitchell DL. 2002. Effective diameter in radiation transfer: General definition, applications, and limitations. *J. Atmos. Sci.* **59**: 2330–2346, doi: 10.1175/1520-0469(2002)059<2330:EDIRTG>2.0.CO;2.
- Morrison H, Gettelman A. 2008. A new two-moment bulk stratiform cloud microphysics scheme in the community atmosphere model, version 3

- (CAM3). Part I: Description and numerical tests. *J. Clim.* **21**: 3642–3659, doi: 10.1175/2008JCLI2105.1.
- Nakajima T, King MD. 1990. Determination of the optical thickness and effective particle radius of clouds from reflected solar radiation measurements. Part I: Theory. *J. Atmos. Sci.* **47**: 1878–1893, doi: 10.1175/1520-0469.
- Pascal N, Manley J. 2009. ‘Calxtract user guide’, Technical report 0605004-NT-UDEV-V01-R06. ICARE: Villeneuve d’Ascq, France. <http://manualzz.com/doc/4141796/calxtract-user-guide> (accessed 15 August 2016).
- Platnick S. 2000. Vertical photon transport in cloud remote sensing problems. *J. Geophys. Res.* **105**: 22919–22935, doi: 10.1029/2000JD900333.
- Platnick S, King MD, Mayer K, Wind G, Amarasinghe N, Marchant B, Arnold G, Zhang Z, Hubanks P, Ridgway B, Riedi J. 2014 ‘MODIS cloud optical properties: User guide for the Collection 6 Level-2 MOD06/MYD06 product and associated level-3 datasets version 0.9 (beta)’, Technical report. NASA Goddard Space Flight Center: Greenbelt, MA.
- Rodgers CD. 1996. Information content and optimisation of high spectral resolution measurements. In *Optical Spectroscopic Techniques and Instrumentation for Atmospheric and Space Research II*, 2830: 136–147. SPIE: Bellingham, WA, doi: 10.1117/12.256110.
- Rodgers CD. 2000. *Inverse Methods for Atmospheric Sounding: Theory and Practice*. World Scientific: Singapore.
- Roebeling RA, Feijt AJ, Stammes P. 2006. Cloud property retrievals for climate monitoring: Implications of differences between spinning enhanced visible and infrared imager (SEVIRI) on Meteosat-8 and Advanced Very High Resolution Radiometer (AVHRR) on NOAA-17. *J. Geophys. Res.: Atmos.* **111**: D20210, doi: 10.1029/2005JD006990.
- Sassen K, Wang Z, Liu D. 2008. Global distribution of cirrus clouds from CloudSat/cloud-aerosol lidar and infrared pathfinder satellite observations (CALIPSO) measurements. *J. Geophys. Res.* **113**: D00A12, doi: 10.1029/2008JD009972.
- Schüller L, Bennartz R, Fischer J, Brenguier JL. 2005. An algorithm for the retrieval of droplet number concentration and geometrical thickness of stratiform marine boundary-layer clouds applied to MODIS radiometric observations. *J. Appl. Meteorol.* **44**: 28–38, doi: 10.1175/JAM-2185.1.
- Sourdeval O, Labonnote LC, Brogniez G, Jourdan O, Pelon J, Garnier A. 2013. A variational approach for retrieving ice cloud properties from infrared measurements: Application in the context of two IIR validation campaigns. *Atmos. Chem. Phys.* **13**: 8229–8244, doi: 10.5194/acp-13-8229-2013.
- Sourdeval O, C-Labonnote L, Baran AJ, Brogniez G. 2015. A methodology for simultaneous retrieval of ice and liquid water cloud properties. Part I: Information content and case-study. *Q. J. R. Meteorol. Soc.* **141**: 870–882, doi: 10.1002/qj.2405.
- Stephens GL. 2005. Cloud feedbacks in the climate system: A critical review. *J. Clim.* **18**: 237–273, doi: 10.1175/JCLI-3243.1.
- Testud J, Oury S, Black RA, Amayenc P, Dou X. 2001. The concept of ‘normalized’ distribution to describe raindrop spectra: A tool for cloud physics and cloud remote sensing. *J. Appl. Meteorol.* **40**: 1118–1140, doi: 10.1175/1520-0450(2001)040<1118:TCOND>2.0.CO;2.
- Tiedtke M. 1993. Representation of clouds in large-scale models. *Mon. Weather Rev.* **121**: 3040–3061, doi: 10.1175/1520-0493(1993)121<3040:ROCILS>2.0.CO;2.
- Waliser DE, Li JLF, Woods CP, Austin RT, Bacmeister J, Chern J, Del Genio A, Jiang JH, Kuang Z, Meng H, Minnis P, Platnick S, Rossow WB, Stephens GL, Sun-Mack S, Tao WK, Tompkins AM, Vane DG, Walker C, Wu D. 2009. Cloud ice: A climate model challenge with signs and expectations of progress. *J. Geophys. Res.* **114**(:): doi: 10.1029/2008JD010015.
- Wang J, Rossow WB, Zhang Y. 2000. Cloud vertical structure and its variations from a 20-year global rawinsonde dataset. *J. Clim.* **13**: 3041–3056, doi: 10.1175/1520-0442(2000)013<3041:CVSAIV>2.0.CO;2.
- Wang C, Platnick S, Zhang Z, Meyer K, Wind G, Yang P. 2016a. Retrieval of ice cloud properties using an optimal estimation algorithm and MODIS infrared observations: 2. Retrieval evaluation. *J. Geophys. Res.: Atmos.* **121**: 5827–5845, doi: 10.1002/2015JD024528.
- Wang C, Platnick S, Zhang Z, Meyer K, Yang P. 2016b. Retrieval of ice cloud properties using an optimal estimation algorithm and modis infrared observations: 1. Forward model, error analysis, and information content. *J. Geophys. Res.: Atmos.* **121**: 5809–5826, doi: 10.1002/2015JD024526.
- Watts PD, Mutlow CT, Baran AJ, Zavody AM. 1998. Study on cloud properties derived from meteosat second generation observations, Final Report 97/181. EUMETSAT: Darmstadt, Germany.
- Watts PD, Bennartz R, Fell F. 2011. Retrieval of two-layer cloud properties from multispectral observations using optimal estimation. *J. Geophys. Res.* **116**: D16203, doi: 10.1029/2011JD015883.
- WCRP. 1986. *A Preliminary Cloudless Standard Atmosphere for Radiation Computation*, WCP-112. International Association for Meteorology and Atmospheric Physics: Boulder, CO.
- Wind G, Platnick S, King MD, Hubanks PA, Pavolonis MJ, Heidinger AK, Yang P, Baum BA. 2010. Multilayer cloud detection with the MODIS near-infrared water vapor absorption band. *J. Appl. Meteorol. Climatol.* **49**: 2315–2333, doi: 10.1175/2010JAMC2364.1.
- Winker DM, Pelon J, Coakley JA, Ackerman SA, Charlson RJ, Colarco PR, Flamant P, Fu Q, Hoff RM, Kittaka C, Kubar TL, Le Treut H, McCormick MP, Mégie G, Poole L, Powell K, Trepte C, Vaughan MA, Wielicki BA. 2010. The CALIPSO mission: A global 3D view of aerosols and clouds. *Bull. Am. Meteorol. Soc.* **91**: 1211–1229, doi: 10.1175/2010BAMS3009.1.
- Yang P, Gao BC, Baum BA, Wiscombe WJ, Hu YX, Nasiri SL, Soulen PF, Heymsfield AJ, McFarquhar GM, Miloshevich LM. 2001. Sensitivity of cirrus bidirectional reflectance to vertical inhomogeneity of ice crystal habits and size distributions for two moderate-resolution imaging spectroradiometer (MODIS) bands. *J. Geophys. Res.: Atmos.* **106**: 17267–17291, doi: 10.1029/2000JD900618.
- Yang H, Dobbie S, Herbert R, Connolly P, Gallagher M, Ghosh S, Al-Jumur SMRK, Clayton J. 2012. The effect of observed vertical structure, habits, and size distributions on the solar radiative properties and cloud evolution of cirrus clouds. *Q. J. R. Meteorol. Soc.* **138**: 1221–1232, doi: 10.1002/qj.973.
- Zhang Z, Platnick S, Yang P, Heidinger AK, Comstock JM. 2010. Effects of ice particle size vertical inhomogeneity on the passive remote sensing of ice clouds. *J. Geophys. Res.: Atmos.* **115**: D17203, doi: 10.1029/2010JD013835.
- Zhang Z, Ackerman AS, Feingold G, Platnick S, Pincus R, Xue H. 2012. Effects of cloud horizontal inhomogeneity and drizzle on remote sensing of cloud droplet effective radius: Case studies based on large-eddy simulations. *J. Geophys. Res.: Atmos.* **117**: D19208, doi: 10.1029/2012JD017655.